J Neurophysiol 94: 2120–2138, 2005.
First published May 31, 2005; doi:10.1152/jn.00117.2005.

Localization and Connectivity in Spinal Interneuronal Networks: The Adduction–Caudal Extension–Flexion Rhythm in the Frog

Philippe Saltiel,[1] Kuno Wyler-Duda,[1] Andrea d'Avella,[2] Robert J. Ajemian,[1] and Emilio Bizzi[1,3]

[1]*Department of Brain and Cognitive Sciences and McGovern Institute for Brain Research, Massachusetts Institute of Technology, Cambridge, Massachusetts;* [2]*Department of Neuromotor Physiology, Istituto di Ricovero e Cura a Carattere Scientifico Fondazione Santa Lucia; and* [3]*European Brain Research Institute, Rome, Italy*

Submitted 1 February 2005; accepted in final form 19 May 2005

Saltiel, Philippe, Kuno Wyler-Duda, Andrea d'Avella, Robert J. Ajemian, and Emilio Bizzi. Localization and connectivity in spinal interneuronal networks: the adduction–caudal extension–flexion rhythm in the frog. *J Neurophysiol* 94: 2120–2138, 2005. First published May 31, 2005; doi:10.1152/jn.00117.2005. We have previously reported that focal intraspinal *N*-methyl-D-aspartate (NMDA) iontophoresis in the frog elicits a motor output, which is organized in terms of its constituent isometric force directions at the ipsilateral ankle and its topography. Furthermore, the associated EMG patterns can be reconstructed as the linear combinations of seven muscle synergies, labeled A to G. We now focus on one of the most common NMDA-elicited outputs, the adduction–caudal extension–flexion rhythm, and examine the relationship between the different force phases in terms of synergies and topography. Two distinct EMG patterns produce caudal extensions, and only one of the two patterns is used at most sites. The key synergy combinations for the two patterns are B + e and D + c (strongest synergies capitalized). These two patterns map at distinct locations in the lumbar cord. Within individual sites rhythms, we find linkages among the synergies used to produce adductions, the onsets of flexions after caudal extensions, and the synergy pattern producing the caudal extensions. For example, the synergy composition of adductions at B + e caudal extension sites is dominated by E + b and at D + c caudal extension sites by C + d. The two types of adductions map at distinct locations, situated between the two caudal extension regions. Specifically the linked patterns of caudal extension–adduction interleave rostrocaudally in a CE2-ADD1-ADD2-CE1 sequence, where 1 and 2 refer to the two pattern types. The implications of this topography and connectivity with respect to motor systems organization and behaviors are discussed.

INTRODUCTION

One question of interest is to characterize the topography of spinal interneuronal networks, and more generally, the neural substrate of different phases of a complex movement.

A related question is whether, for a single phase of movement, there could be one or a few spinal cord regions primarily responsible for its production. Knowledge regarding this question is limited. For example, in the cat, the existence of distinct interneuronal systems producing extensions is suggested by the lack of spatial facilitation of vestibular inputs and inputs from group I afferents from knee and ankle extensors, two classes of inputs separately able to excite extensors (Leblond and Gossard 1997; Leblond et al. 2000). However, very little is known about a potential topographic segregation of these interneurons. It is also not known to what extent the EMG patterns underlying extensions produced by these different inputs differ.

Similarly, although central pattern generators (CPGs) intrinsic to the spinal cord are known to exist, they are still not well understood in terms of localization of function (encoding of specific phases) or specific connectivity that might underlie the construction of rhythms. In fact CPGs have long been considered to be diffusely organized (Kjaerulff and Kiehn 1996), apart for a rostrocaudal gradient of excitability (Bertrand and Cazalets 2002). In the turtle, it has been difficult to distinguish an interneuronal topography related to specific types of wipe or to specific phases shared by different wipes (Berkowitz 2001a,b), even though evidence for modularity has been found for example by examining hip extensor deletions (Stein and Daniels-McQueen 2002, 2004). Other recent research, however, points out at the possibility of a more precise topography of spinal cord interneuronal function (reviewed in Tresch et al. 2002). For example, in cat locomotion, focal microinjections have revealed the specific importance of mid-lumbar segments in rhythmogenesis (Marcoux and Rossignol 2000). In mudpuppy forelimb locomotion, stimulation and recording studies suggest a significant tendency for flexor-related interneurons to be located rostral to extensor-related interneurons in the cervical cord (Cheng et al. 1998, 2002). The recent distinction between different categories of descending commissural interneurons in rodent locomotion constitutes evidence for the possibility of identifying specific patterns of connectivity in the spinal cord (Butt and Kiehn 2003).

Similarly, the topographic organization of the motor systems remains incompletely understood for the motor cortex. While it is clear that a small cortical locus is able to activate several muscles innervated by different motoneuron pools through divergence, and that this changes across the cortex (Park et al. 2001, 2004; Schieber 2001), the role of the extensive intrinsic horizontal connections between motor cortical regions in the organization of movement remains unclear. It has been suggested that these connections may be involved in coordinating the different phases of a movement (Keller 1993).

One of the main classes of rhythms obtained with focal NMDA iontophoresis in the spinal frog is the adduction–caudal extension–flexion (ADD-CE-FL) rhythm. Among these force directions, *N*-methyl-D-aspartate (NMDA) can also pro-

Address for reprint requests and other correspondence: P. Saltiel, MIT, Dept. of Brain and Cognitive Sciences, McGovern Inst. for Brain Research, 77 Massachusetts Ave., E25-526, Cambridge, MA 02139 (E-mail: saltiel@mit.edu).

The costs of publication of this article were defrayed in part by the payment of page charges. The article must therefore be hereby marked "*advertisement*" in accordance with 18 U.S.C. Section 1734 solely to indicate this fact.

duce adductions and caudal extensions as single tonic forces. These tonic forces map at distinct locations, which include two different locations for caudal extensions. The sites producing the ADD-CE-FL rhythm (or fragments of it) in turn map close to these locations, suggesting that the neural substrate of the tonic regions for caudal extension and adduction participate in the construction of this rhythm (Saltiel et al. 1998).

In this paper, we studied the synergy combinations underlying the EMG patterns that produce the caudal extensions and adductions in particular, and we map these patterns onto the spinal cord. Our results emphasize that there are two distinct types of caudal extensions and that these are linked to different types of adduction. We find correspondingly distinct topography for the different types of caudal extensions and adductions. Mapping the linked patterns further suggests that connectivity between distantly located rather than between adjacent cord regions underlies the rhythm construction. Our results therefore support a topographic organization of spinal motor interneuronal systems and cast it in the framework of connectivity between specific cord regions to orchestrate different phases of a complex movement. These results should be behaviorally relevant, because caudal extensions are part of many natural behaviors in the frog, such as swimming, jumping, hind-limb wipe, and some types of kicks.

METHODS

Surgery

This has been described in detail previously (Saltiel et al. 1998, 2001). The frogs used in this paper are the same as those in our 2001 paper ($n = 10$), except for the maps where the frogs of the 1998 paper ($n = 13$) were used in addition. A few illustrations (Figs. 1*B* and 3*A*, right) also come from the 1998 set of frogs. All procedures were approved by the Animal Care Committee at Massachusetts Institute of Technology. Briefly, after anesthesia with 1 ml of Tricaine methanesulfonate subcutaneously supplemented by ice, the frog (*Rana catesbeiana*) was spinalized at the level of the obex. Twelve muscles of the hindlimb were implanted with bipolar EMG electrodes: rectus internus (RI), adductor magnus (AM), semitendinosus (ST), sartorius (SA), vastus internus (VI), rectus anterior (RA), vastus externus (VE), iliopsoas (IP), biceps femoris (BF), semimembranosus (SM), gastrocnemius (GA), peroneus externus (PE). Most of these muscles are biarticular. However, their actions have been characterized as force fields by electrically stimulating the individual muscles and recording the forces they produce at the ankle in different isometric limb configurations (Loeb et al. 2000). Accordingly, the RI and AM force fields are hip extensor and knee flexor, SM hip extensor, ST predominantly knee flexor, IP and RA hip flexor, VI, VE and PE knee extensor, BF and SA hip flexor and knee flexor. GA is a knee flexor and plantarflexor. After laminectomy of the 4th, 5th, and 6th vertebrae, the dura was opened with electrocautery and scissors and the pia with fine scissors to expose the dorsal surface of the right side of the lumbar spinal cord from above the 7th root to below the 10th root. A detailed drawing was made of the exposed spinal cord vasculature and dorsal root entry zones, which later served to document the points of entry of the micropipette within each segment.

Iontophoresis

A 2.5-μm tip three-barrel pipette was used. Besides the NMDA barrel, one barrel was for current balancing, and the third was available for electrical stimulation. Another pipette was glued to the side for recording. NMDA was iontophoresed with parameters (-100 nA, for a maximum of 30 s or up to the time of onset of EMG activity), which should be associated with a spread of 150–270 μm radius by the average time of onset of EMG activity (Saltiel et al. 1998).

Data recording

The spinalized frog was immobilized on a moistened molded stand with body and pelvis clamps. The ipsilateral hindlimb was placed in a force sensor apparatus and held isometric in a standard position (hip and knee angles of 74° and 79°, ankle at the same vertical position as the hip). EMGs, amplified 25,000 times, and forces in three dimensions were simultaneously recorded at 2,000 Hz for 60 s starting with the onset of NMDA iontophoresis. In one frog (F162), they were recorded for two 60-s periods separated by a brief interruption. NMDA was generally applied at depths of 500, 800, and 1,100 μm, 200–400 μm from the midline. Our previous study has shown the focality and the reproducibility of this method and provided evidence from simultaneously applied TTX that the effects of NMDA represent interneuronal stimulation (Saltiel et al. 1998).

Data analysis

After down-sampling simultaneously the recorded forces and EMGs to 1,000 Hz, we parsed them independently into responses of stable force direction and of stable EMG pattern. We intersected the times derived from the force and EMG parsing to further subdivide the force intervals, both stable and unstable, on the basis of any intervening transition from the EMG parsing. This is necessary because a given force direction may be produced by more than one EMG pattern.

Force angle parsing

The first second of each force record was subtracted as the passive force to yield the active force. For each sample, the horizontal force direction was computed with the notation: 0° rostral, ±180° caudal, 90° lateral, −90° medial. The force angle was further down-sampled by retaining every 10th value and smoothed using Tukey's method (1977), which we adapted for circular data. Forces were parsed using a computer algorithm (Saltiel et al. 1998), which defined stable forces as intervals, where each sample differed by no more than 4° from the sample 130 ms earlier, and had a magnitude above the noise level of 2 force units (22.24 mN). Stable forces separated by gaps of <160 ms were subsequently bridged into a single stable force, because in force angle plots, no transition between clearly different stable force angle levels occurred faster than in 160 ms. Visual inspection of stability of automatically detected responses showed a very good agreement. For weak responses, corrections were sometimes necessary when excessively parsed. Finally we multiplied the onset and offset times of all stable force direction intervals by 10 and subtracted 9 ms to return to the same time scale as the EMGs. This corrected for the down-sampling step where we had retained every 10th value of the force angle.

EMG parsing

The first second of the EMG records was averaged and subtracted as the baseline to remove any possible tonic noise bias. The records were parsed as successive EMG responses, using interactive software from Matlab. Any visually significant change in the ongoing EMG activity from the 12 muscles was marked as a different response. In this way, we hoped to avoid forced grouping of muscles. We have shown previously that this method of parsing did not introduce a bias when subsequently applying the synergy extraction algorithm to EMG data (Saltiel et al. 2001).

Intersection of EMG and force angle parsing

We subtracted 50 ms from the force times to take in account the EMG to force delay. A program was written to intersect the force times with those from the EMG parsing, as explained previously. Thus an individual stable force interval could typically consist of several parsed EMG responses (see Figs. 1 and 4). To avoid excessive parsing, force and EMG parsing lines that were <15 ms apart were fused into a single line at the time of the EMG line.

Determining the average force and EMGs during each individual response

For each EMG response with a stable force direction, the average force angle was determined. Because force angle values ranged from −180 to 180°, it was not possible to simply average the individual sample angle values (e.g., the average of +175 and −175° should be a caudal force of ±180°, not 0°). Therefore we normalized the response consecutive force samples to unit vectors ($Fx^2 + Fy^2 = 1$), and these will contribute equally to the calculated average force direction. The average force angle was then obtained with the notation as above by computing the angle between the summed *Fx* and *Fy* values of the unit vectors (taking the arctangent of these sums). Force magnitude was computed by averaging the square roots of the sum of squares of *Fx* and *Fy* across the force samples of the response. A histogram of the distribution of the force directions showed clusters similar to those previously reported (Saltiel et al. 1998). On the basis of this histogram, we defined a caudal extension as ≥165 or ≤−142.5°, adduction as ≤−52.5 and ≥−97.5°, and flexion as ≤0 and ≥−45°.

EMGs were rectified, and the first second of the records was subtracted again to remove any oscillatory noise about zero that could have remained uncorrected after the first unrectified baseline subtraction. Each rectified EMG response associated with a stable or a changing force direction was averaged between its time of onset and offset to a single value for each of the 12 muscles. In each frog, these EMG values were subsequently normalized for each muscle to the maximal EMG activity recorded in that muscle from any response from that frog. This was done to correct for possible electrode sampling differences between frogs.

Reconstruction of EMG responses as synergy combinations

To characterize the EMG patterns underlying caudal extensions, adductions, and flexions, we want to express them as combinations of the seven synergies (labeled A–G) that we have extracted in previous work from all NMDA-elicited EMG responses (without consideration of force direction). We have also previously reported that preferred combinations of the seven synergies A–G exist that can be found in a simple manner by extracting a smaller set of four synergies and expressing them as combinations of the seven synergies (Saltiel et al. 2001). This method has the advantage that it becomes possible to describe the EMG patterns with only a small number of coefficients of activation (≤4) of these synergy combinations.

Synergy combinations for caudal extensions

We considered the EMG responses associated with stable force directions ≥97.5 or ≤−142.5°, which comprises all extensions (both caudal and lateral). To these we added the EMG responses associated with a transition to these stable force directions from a different stable force direction; the reason for including these responses is because we generally observed similar EMGs when the limb was driven to a new stable force direction as when this direction was maintained. We applied 150 iterations of our previously described nonnegative least-squares factorization algorithm (Saltiel et al. 2001; Tresch et al. 1999) to extract four synergies whose linear combinations best accounted for these responses and to simultaneously find the coefficients of synergy activation for these responses. To express these four synergies as combinations of the seven NMDA synergies (A–G), we used the same algorithm, initialized with the seven synergies, and without iteration, to fit the four synergies. These synergy combinations are A, B + e, D + c, and F + G, where the capital letters indicate the more strongly activated synergies (see Fig. 2).

Synergy combinations for adductions and flexions

In a similar way, we considered the EMG responses associated with stable force directions ≤−52.5 and ≥−97.5° or ≤0 and ≥−45°, which comprises all adductions and flexions, to which we again added the EMG responses associated with a transition to these stable force directions from a different stable force direction. From these responses we again extracted four synergies and their coefficients of activation and expressed the four synergies as combinations of the seven NMDA synergies. These synergy combinations are A + F + c, E + b, C + d, and F + b (see Fig. 5, *A* and *B*).

Criteria for identifying a site with caudal extensions of pure B + e or D + c type

We determined the subset of spinal cord sites where the NMDA-elicited caudal extension responses remained of the B + e or D + c type throughout the record, i.e., conformed to a single pattern. This was done by plotting for each site the coefficients of the synergy combination B + e against those of the synergy combination D + c, as they reconstructed the stable caudal extension responses as well as the responses bringing the limb to a stable caudal extension from another stable force direction, and fitting a least squares line to the plotted coefficient data. Because synergy combinations B + e and D + c are independent variables, we used a perpendicular offset least squares fitting method that minimizes the sum of squares of the perpendicular distances from the data points to the fitted line, rather than the distances along the *y*-axis (Weisstein 2003). We also determined the intercept of the fitting line. We are particularly interested in sites with least squares lines close to the B + e or D + c axes. The distributions of perpendicular offset least squares lines slopes and intercepts were examined in histograms to establish criteria for saying that a site's caudal extensions remained of pure B + e or D + c type throughout (see Fig. 3, *B* and *C*).

Adduction composition at pure B + e and D + c caudal extension sites

To examine for possible linkages between the synergy composition of caudal extensions and adductions, we averaged at each pure B + e and each pure D + c caudal extension site the coefficients of the four synergy combinations, reconstructing the EMG responses producing a stable adduction or bringing the limb to a stable adduction from another stable force direction. Each average was expressed so that the sums of the four coefficients equaled 100% (see Fig. 5*C*). A MANOVA was run to determine whether there was a statistically significant difference between the adduction synergy composition averages from B + e versus D + c caudal extension sites.

Composition of flexion onset after caudal extension at pure B + e and D + c caudal extension sites

We first compared the synergy composition of flexions after caudal extensions at B + e versus D + c caudal extension sites. Because flexions are typically produced by a multiphasic sequence of EMGs, we focused on the flexion onsets. They were defined as beginning when the force direction changed toward a stable flexion from a stable caudal extension and ending when the line joining the synergy composition of successive responses changed direction by >22.5° in

the four-dimensional space of the four synergy combinations reconstructing the flexions. A change in line direction over three successive responses when two are very close would not be meaningful. Thus if the first response was away from the origin <5% of the range (maximum value of the flexion responses coefficients at the site), the first of the consecutive lines began with that first response instead of from the origin. Similarly, when two consecutive responses were separated by <5% of the range, the change in line direction was examined with the next consecutive response >5% away in distance. Once the responses constituting the onsets of flexions after caudal extensions were determined, the four synergy coefficients reconstructing these responses were averaged at each site in a similar way to the adductions above, and each average subsequently was expressed so that the sums of the four coefficients equaled 100% (see Fig. 7*A*).

Combined adduction and flexion onset composition at pure B + e and D + c caudal extension sites

At each site where caudal extensions were of pure B + e or D + c type and where NMDA also elicited both adductions and flexions, the average synergy composition of the adductions and of the flexion onsets, each expressed so that the sums of the four coefficients equaled 100%, were averaged together (see Fig. 7*F*). The combined adduction/flexion onset synergy composition averages from B + e versus D + c caudal extension sites were statistically compared by MANOVA.

Mapping initial caudal extension sites

To map the caudal extension B + e and D + c patterns, we determined among the caudal extension sites of pure B + e or D + c type, the subset where a caudal extension was the first force produced by NMDA iontophoresis. We mapped this subset with two different symbols according to whether caudal extensions were of the B + e or the D + c type. To increase the number of mapped sites, we added another group of frogs (the one reported in Saltiel et al. 1998). For adding initial caudal extension sites from these frogs to the map, we similarly requested that the caudal extensions remained of the pure B + e or D + c type throughout the record, as assessed by the perpendicular offset least-squares method outlined above.

Mapping initial adduction sites

To map the adductions of the type linked to B + e or to D + c caudal extensions, we determined the sites where NMDA iontophoresis produced an adduction as the initial force. The earlier group of frogs was again included. For each initial adduction site, the four synergy coefficients reconstructing the EMG responses of the initial adduction were averaged, and the average was expressed so that the sums of the four coefficients equaled 100%. Sites where none of the initial adduction EMG responses produced an adduction force greater than the noise level of two force units in magnitude (22.24 mN, criterion of Saltiel et al. 1998) were excluded. We used the k-means clustering algorithm (Hartigan and Wong 1979) to cluster the initial adduction synergy compositions in two groups, according to whether they resembled most the adductions from sites with B + e caudal extensions or resembled most the adductions from sites with D + c caudal extensions, which were therefore chosen as the two initial k-means centers (Fig. 5*C*). Initial adduction sites whose initial adduction synergy composition was at a large distance (computed as 1 − normalized dot product) from both of these k-means centers were excluded as outliers before clustering (Fig. 9, *left inset*). The k-means algorithm assigns each data point (here an initial adduction synergy composition) to the cluster with which center it has minimal distance. In the next step, it recalculates the centers by averaging the members of its cluster. This process is repeated until the mean of the distances between the elements of the clusters and their centers decreases by <0.1%. Once the clustering done, we mapped with two different symbols the initial adduction sites belonging to the two clusters of initial adduction synergy composition. The hypothesis that, within the seventh to ninth root segments, the initial adductions of the type linked to B + e caudal extensions map more rostrally than the initial adductions of the type linked to D + c caudal extensions was tested statistically both by Mann-Whitney and by *t*-test.

Mapping linked synergies

To study the topography of linked synergies, we represented those synergies that are linked in the rhythms with the same symbol. Thus we combined in the same map the sites producing either initial caudal extensions of D + c type or initial adductions of the type linked to D + c caudal extensions, all shown with the symbol ●, and the sites producing either initial caudal extensions of B + e type or initial adductions of the type linked to B + e caudal extensions, all shown with the symbol ○. We focused on whether the spinal cord showed several regions of either ● or ○ predominance, which could be thought of as constituting a network of ● or ○ synergies linked in the rhythms. This was determined by two methods: visual inspection and Gaussian analysis.

With visual inspection, we traced parsimonious boundaries around nonoverlapping regions containing a predominance of ● or ○ sites (Fig. 10*A*).

In the second method, we smoothed the topography by representing each site as a Gaussian (area under the curve equal to 1), according to the equation $f(x) = 1/[\sigma \sqrt{(2\pi)}] \exp[-(x - s)^2/2\sigma^2]$ (Weisstein 2004), where s is the center of the Gaussian at the site's rostrocaudal location, σ is its width, and x is a continuous variable along the rostrocaudal extent of the lumbar cord, which like s and σ is expressed as a percentage of mid-DR6 (0%) to mid-DR10 (100%). We used σ values of 3, 2.5, and 2% as Gaussian widths. The σ of 3% seems reasonable, given that the SD of the difference between location measurements derived from the spinal cord diagram documenting the pipette site of entry and postmortem microdrive measurements was equal to 7.46% of mid-DR7 to mid-DR9 (n = 8 DR7-DR9 sites), which corresponds to 3.45% of mid-DR6 to mid-DR10. We then summed the Gaussians of the ● and ○ sites separately, normalized the sums to an equal number of sites, and plotted them as two curves along the length of the lumbar cord to identify the location of the peaks of ● and ○ topography. The intersections of the two curves between these peaks define the boundaries between regions of ● and ○ predominance (Fig. 10*B*). With σ of 2%, there were smaller peaks between the major peaks, resulting in more intersections between the two curves. To define the boundaries, we assigned the regions of weak ● or ○ predominance between the major peaks, to the neighboring major peak of the same predominance.

RESULTS

Two distinct EMG patterns produce caudal extensions

Figure 1 shows representative examples of two different patterns producing caudal extensions, which were initially identified by visual inspection. While they share activation of GA,pe, one pattern (Fig. 1*A*) also activates muscles ri,SM, ip,ra,BF,VE (capital letters for the more strongly activated muscles), whereas the other pattern (Fig. 1*B*) also activates muscles RI,AM,SM,st,ip,SA. Thus with respect to the seven synergies extracted from all NMDA EMG patterns (Saltiel et al. 2001; reproduced in Fig. 2*B*), one pattern appears defined by the activation of synergies D + c (capital letters for the more strongly activated synergies) and the other pattern by the activation of synergies B + e, whereas the two patterns share synergy A.

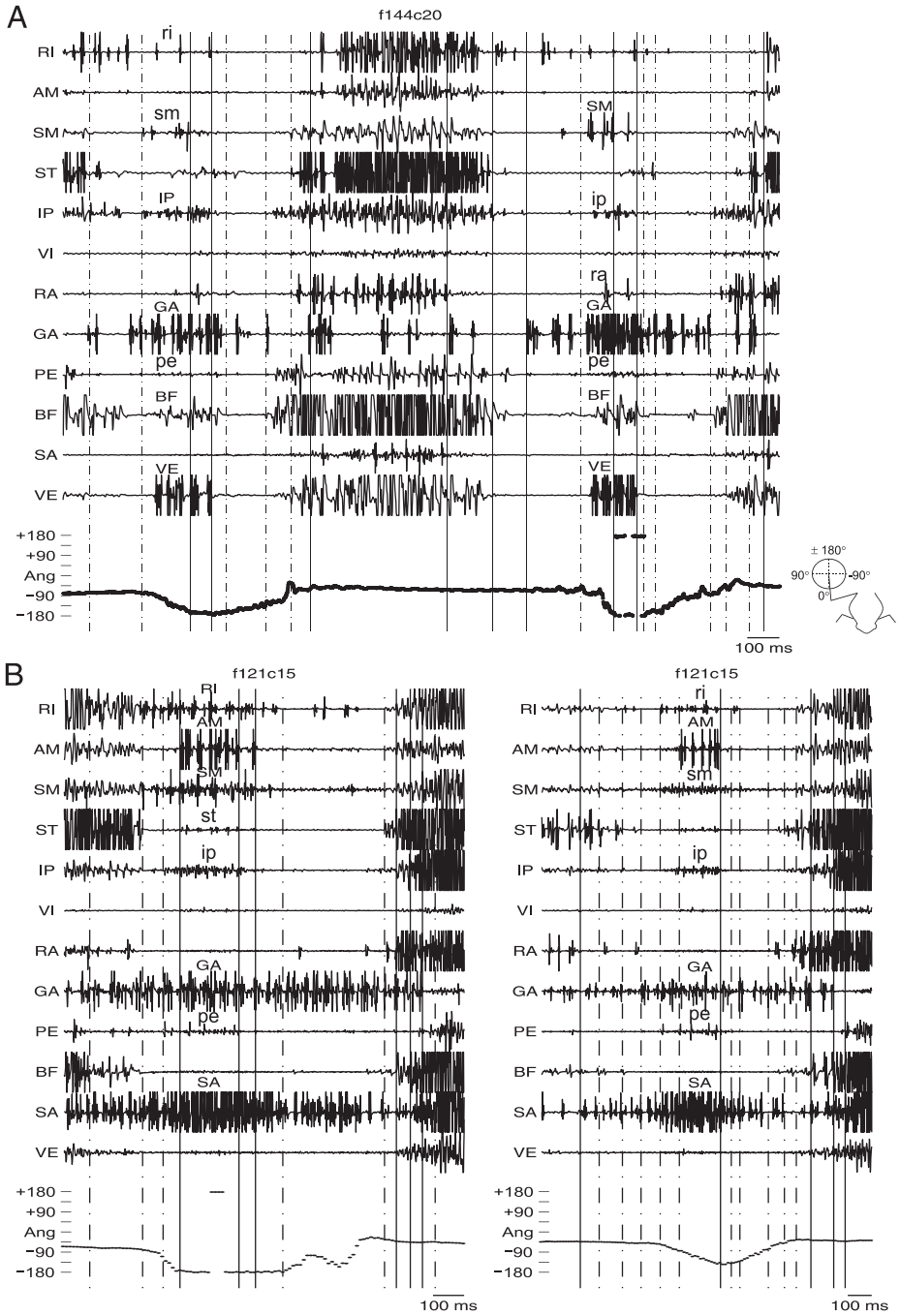

FIG. 1. Two caudal extension EMG patterns. *A* and *B*: *N*-methyl-D-aspartate (NMDA)-elicited EMGs and forces at 2 different sites in 2 different frogs (f144c20 and f121c15). Recorded muscles were as follows: RI, rectus internus; AM, adductor magnus; SM, semimembranosus; ST, semitendinosus; IP, iliopsoas; VI, vastus internus; RA, rectus anterior; GA, gastrocnemius; PE, peroneus; BF, biceps femoris; SA, sartorius; VE, vastus externus. Angle of force direction in the bottom trace of each panel is oriented with respect to the frog as shown in the *inset*. Vertical lines result from the intersection of the parsing of the EMGs and forces. Periods of stable force direction begin as a full line replaces dashed lines and end with resumption of a dashed line. *A*: 2 consecutive caudal extensions (force angle changing toward ±180°) recorded 24 s after onset of an adduction–caudal extension rhythm elicited by NMDA at a site located rostrocaudally 37% within the 8th to 9th root segment at a depth of 900 μm. *B*: 2 caudal extensions recorded 10 and 23 s after onset of an adduction–caudal extension–flexion rhythm elicited by NMDA (2nd caudal extension was actually short by 2.5° of the –142.5° criterion) at a site located rostrocaudally 54% within the 7th to 8th root segment at a depth of 580 μm. Main muscles activated during each caudal extension are labeled, with the more strongly activated muscles in capital letters. Note that some muscles are shared between the 2 different EMG patterns producing caudal extensions (GA,pe,SM in *A* and *B*), whereas others are uniquely part of 1 or the other pattern (VE,BF in *A*; AM,SA in *B*). On the other hand, within the panels from each site (f144c20 and f121c15), the EMG pattern is quite reproducible between the 2 shown caudal extensions.

To quantify our impression of two distinct caudal extension patterns, we first determined the coefficients of the above synergy combinations (D + c and B + e) as they reconstruct the caudal extension data. This was done simply by extracting four synergies from the subset of extension (caudal and lateral) force directions (Fig. 2*A*) and reconstructing them as combinations of the seven synergies extracted from all NMDA EMG responses (Fig. 2, *B* and *C*). This technique reliably identifies which synergies preferentially combine to produce the examined data, here extensions (Saltiel et al. 2001). The four combinations are A, D + c, B + e, and F + G (Fig. 2, *A* and *C*), and together they reconstruct 89% of the variance of the extension data. Note that the first three combinations essentially correspond to those identified above by visual inspection. Coefficients of activation in the reconstruction of extensions indicate that the fourth combination is not used for caudal extensions (but rather for lateral extensions).

We can now evaluate the composition of caudal extension responses in terms of the two EMG patterns described in Fig. 1 by plotting the coefficients of activation of the B + e versus D + c synergy combinations for these responses. Figure 3*A, left*, shows a representative example of a site where caudal extensions were of the pure B + e type (no activation of D + c) and Fig. 3*A, right,* of a site where all caudal extension responses were of the pure D + c type (no activation of B + e). Because we are interested in the topography of these caudal extension patterns, we did such plots on a site-by-site basis for each site where NMDA-elicited force directions included caudal extensions.

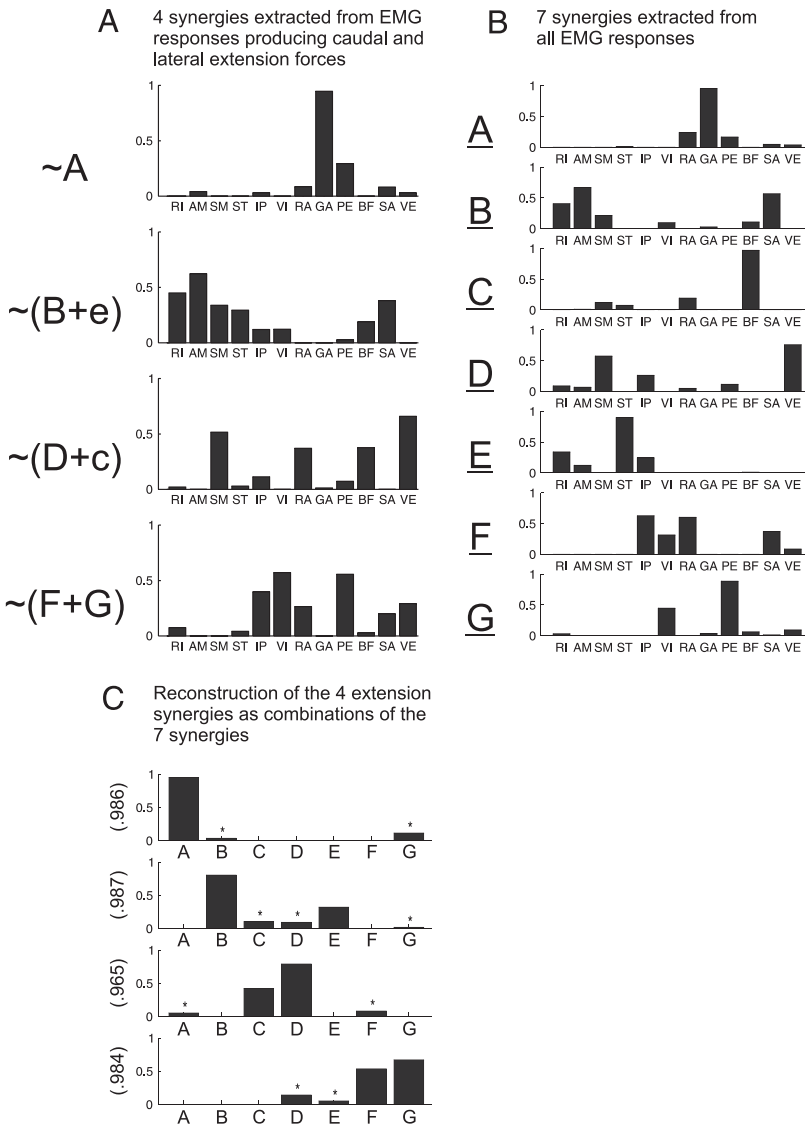

FIG. 2. Four synergies extracted from extensions, and expressed as combinations of the 7 synergies extracted from all EMG responses. *A*: 4 synergies extracted from caudal and lateral extensions. *B*: 7 synergies extracted from all EMG responses, labeled A to G (reproduced from Saltiel et al. 2001). *C*: 4 synergies of *A* formally reconstructed as linear combinations of the 7 synergies of *B*. *Synergies that contributed little to a combination (coefficients of activation between 0 and 0.15). These are, however, included in the computation of the normalized dot product on the ordinate that indicates the quality of the fit provided by each combination. Results of this reconstruction are summarized leftward of the 4 synergies of *A* the 4 synergies of A (A, B + e, D + c, F + G, where capital letters indicate the more strongly activated synergies). In *A*, the 2 key synergy combinations that distinguish between the 2 caudal extension EMG patterns shown, respectively, in Fig. 1, *B* and *A*, are B + e (RI,AM,SM,ST,SA) and D + c (SM,RA,BF,VE). Synergy A (GA,pe) is shared between the 2 patterns. Combination F + G is of little relevance to caudal extensions; it is used for lateral extensions.

To quantify the degree to which *all* caudal extension responses elicited from a site conformed to a pure type, we computed the slope and minimum intercept of a perpendicular offset least-squares line, fitted to the plotted coefficients. A perpendicular offset is used because the B + e and D + c coefficients are two variables on an equal footing, rather than one being dependent on the other (see METHODS). The perpendicular offset lines are shown as dotted lines for the two sites of Fig. 3*A*. In Fig. 3*B*, the distribution of 46 perpendicular offset slopes from sites with caudal extensions is shown in a semicircular histogram, where slopes parallel to the Be axis point upward and slopes parallel to the Dc axis point to the right. This histogram suggests that most caudal extension sites belong to two clusters: a larger one where caudal extensions remain throughout the rhythm of pure B + e type, and a smaller one where they remain of pure D + c type. One still needs to exclude from these a few sites where the intercept is large, because even for perpendicular offset least-squares lines nearly parallel to the B + e or D + c axis, a large intercept would indicate that the caudal extensions result from a mixture of the two synergy combinations. The distribution of the absolute values of intercepts (see METHODS) is shown in Fig. 3*C*, with the arrow indicating the cut-off value for a large intercept. On the basis of these slope and intercept criteria, caudal extensions at 24/45 sites remained of pure B + e type and at 8/45 sites of pure D + c type (1 site where the caudal extension pattern changed from a pure B + e to a pure D + c pattern with time, as shown in Fig. 7, *B* and *C*, contributed 2 values). Thus at 71% (32/45) of the sites where NMDA-elicited forces included caudal extensions, the latter were consistently produced by one or the other of these two distinct EMG patterns.

Linkages between caudal extensions and adductions

We can now examine whether there is a difference between the EMG patterns of adductions elicited from sites where the caudal extensions are of the B + e type as opposed to the D + c type. This is to see whether there is a linkage between the EMG pattern used in one phase (caudal extension) of the rhythm and the pattern used in another phase (adduction). Together with topography, this would have implications about the modular construction of spinal cord rhythms.

We use the 32 above sites with pure caudal extension EMG patterns. To the groups of 24 B + e and 8 D + c caudal

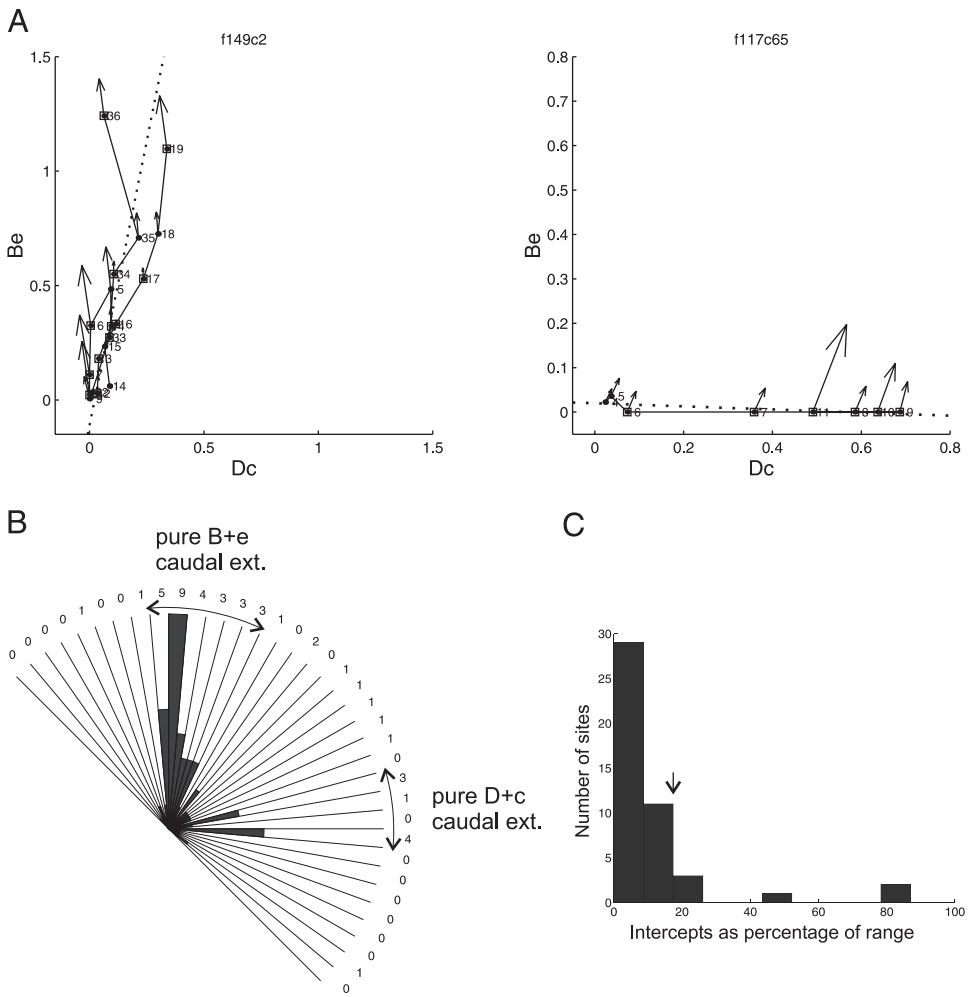

FIG. 3. Caudal extensions elicited from individual sites retain throughout the same underlying B + e (Be) or D + c (Dc) EMG pattern at a majority of sites. *A*: examples of sites where the EMG responses (associated with 3 caudal extensions at site f149c2, and a single caudal extension at site f117c65) remain of the Be or Dc type, respectively. Number labels on the responses identify the consecutive EMG responses producing the caudal extensions (2–9, 14–19, 32–36 f149c2, 4–11 f117c65). Arrows show the average force direction during each response, oriented with respect to the frog as in the *inset* of Fig. 1. Squares indicate those responses where the force direction remained stable. Coefficients of activation of synergies Be and Dc as they reconstruct the caudal extension EMG responses are plotted against one another. Dotted lines show fitting of the data by perpendicular offset least-squares lines. The proximity of these lines to the *y*- (Be) and *x*- (Dc) axes for data plotted on the *left* and *right,* respectively, indicates that caudal extension responses remain of a pure Be and Dc type at these 2 sites, respectively. *B*: distribution of slopes of perpendicular offset least-squares fits to the Be vs. Dc plots from 45 sites where NMDA elicited caudal extensions. Semicircular angular histogram is built from expressing slopes between –1 and $+\infty$ as their arctangent (atan) and slopes between –1 and $-\infty$, as 180° + atan. In this way, there is no discontinuity in the histogram for slopes close to the orientation of the Be axis. A slope parallel to the Dc axis points right in the histogram; a slope parallel to the Be axis points up. Bins are of 5° width, and number of sites in each bin is indicated. One site where the caudal extension pattern changed from Be to Dc with time (see Fig. 7, *B* and *C*) contributed 2 slope values: 1 for the Be and 1 for the Dc portion of its caudal extension data. Circular arcs indicate that, at most sites where NMDA elicits caudal extensions, these remain of pure Be or Dc type. *C*: distribution of absolute intercept values of perpendicular offset least-squares fits to the Be vs. Dc plots from the same 45 sites. Intercepts, chosen as the smaller one in absolute value of the *y*- or *x*-intercept, are expressed as a percentage of the range, where range corresponds to the largest synergy coefficient (Be or Dc) among the site's plotted responses. Vertical arrow indicates chosen cut-off of 17.4%, above which the intercept is considered too large for a site to qualify as eliciting pure Be or Dc caudal extensions, irrespective of slope of least-squares fit.

extension sites, we added 2 sites to each where the EMG pattern, although mixed, clearly started respectively with B + e preceding D + c or with D + c preceding B + e in the individual caudal extensions. At 16 of the 26 B + e and at 8 of the 10 D + c caudal extension sites, NMDA also elicited adductions.

Figure 4*A* is a representative example of an adduction from a B + e caudal extension site, and it is produced by ri,ST,RA, GA,bf, with some other muscles (am,sm,vi,pe,ve) weakly contributing. With respect to the seven synergies extracted from all NMDA EMG patterns (Fig. 2*B*), this pattern would correspond

FIG. 4. Two adduction EMG patterns. *A* and *B*: show the NMDA-elicited EMGs and forces at 2 different sites in 2 different frogs (f160c17 and f162c58). Angle of force direction in the bottom trace of each panel; vertical full and dashed lines as explained in Fig. 1. *A*: adduction–caudal extension–flexion–adduction sequence elicited by NMDA from a site located rostrocaudally 54% within the 7th to 8th root segment at a depth of 780 μm. *B*: tonic adduction from a site located rostrocaudally 10% within the 8th to 9th root segment at a depth of 1,250 μm; continued recording from this site showed a caudal extension–flexion rhythm. Main muscles activated during adductions are labeled, with the more strongly activated muscles in capital letters. Note that some muscles are shared between the 2 different EMG patterns producing adductions (ri,ST in *A* and *B*), whereas others are primarily part of 1 or the other pattern (RA,GA in *A*, BF in *B*). Corresponding to differences in EMG patterns underlying adductions in *A* and *B*, caudal extensions from the *A* site were of Be type (see Fig. 6*A* from the same site), whereas caudal extensions from the *B* site were largely of Dc type (data not shown).

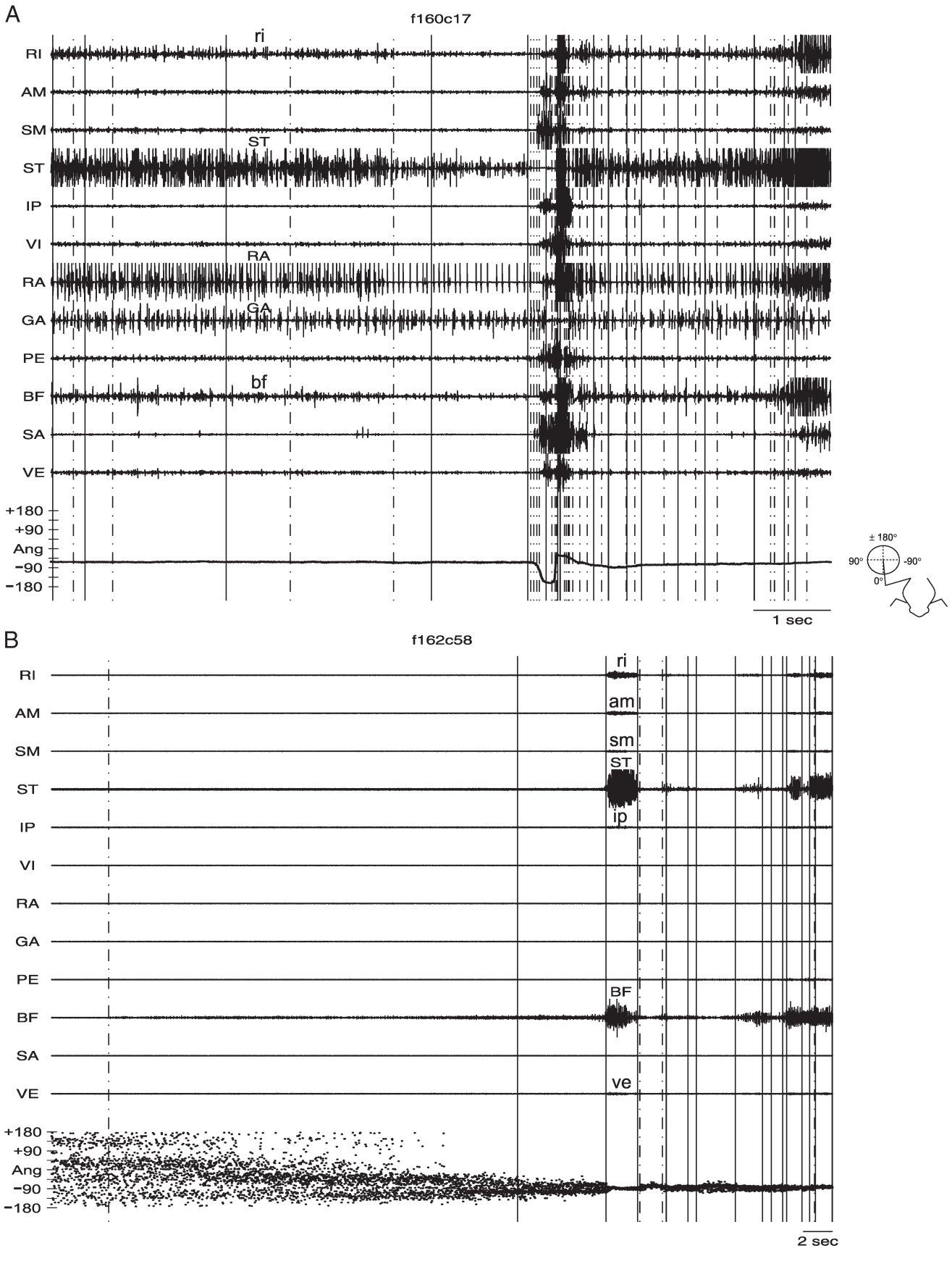

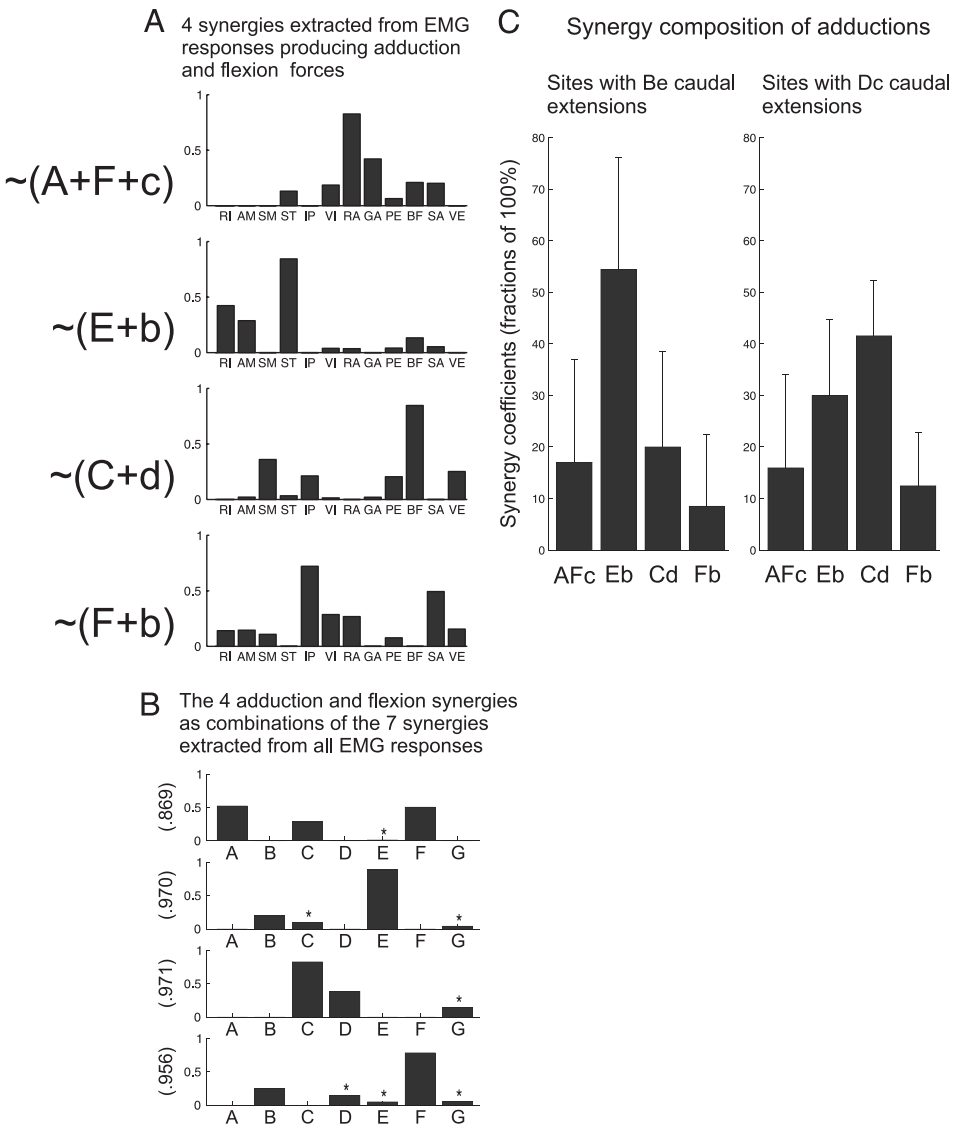

FIG. 5. Synergy composition of adductions from sites eliciting Be vs. Dc caudal extensions. *A*: 4 synergies extracted from adductions and flexions. *B*: 4 synergies of *A* formally reconstructed as linear combinations of the 7 synergies of Fig. 2*B*. *Synergies that contributed little to a combination (coefficients of activation between 0 and 0.15). These are, however, included in the computation of the normalized dot product on the ordinate that indicates quality of the fit provided by each combination. Results of this reconstruction are summarized leftward of the 4 synergies of *A* (A + F + c, E + b, C + d, F + b, where capital letters indicate the more strongly activated synergies). *C*: average synergy composition of adductions, expressed in terms of the 4 synergies of *A*, from sites where NMDA elicited pure Be or Dc caudal extensions (according to our least-squares fit criteria in Be vs. Dc plots) and also elicited adductions. At each site, the average synergy composition of adduction responses was computed and subsequently expressed with the 4 coefficients summing to 100%. Results were averaged for the 2 groups of caudal extension sites (Be, $n = 16$; Dc, $n = 8$). Height of bars indicates average, and thin bars indicate SD.

to the activation of synergies E + A + F + b + c. Figure 4*B* is a representative example of an adduction from a D + c caudal extension site, and it is produced by ri,am,sm,ST,ip,BF,ve. This pattern would correspond to the activation of synergies E + C + b + d.

In a similar way to extensions, we extracted four synergies from the subset of adduction and flexion force directions (Fig. 5*A*) and reconstructed them as combinations of the seven synergies extracted from all NMDA EMG responses (Fig. 5*B*). The four synergy combinations are A + F + c, C + d, E + b, and F + b (Fig. 5, *A* and *B*), and together they reconstruct 85% of the variance of the adduction and flexion data. Note that the first three combinations essentially correspond to those that would enter in the patterns identified above by visual inspection (i.e., E + b and A + F +c in the 1st pattern, E + b and C + d in the 2nd pattern). Coefficients of activation for the adduction/flexion data indicate that the fourth combination is not much used for adductions (but rather for flexions).

While the EMG patterns producing adductions do not always conform to the rather pure types depicted in Fig. 4, they do tend to correspond more closely to one or the other pattern, in relation to the type of caudal extensions elicited from the same site. This can be appreciated by averaging the coefficients of the four synergy combinations as they reconstruct the adductions of B + e caudal extension sites and comparing them to the averaged coefficients for the adductions of D + c caudal extension sites (see METHODS). These averages are shown in Fig. 5*C*. At B + e caudal extension sites ($n = 16$), the main synergy combination entering in the composition of adductions is E + b. At D + c caudal extension sites ($n = 8$), mainly the C + d and E + b synergy combinations together reconstruct adductions, with a tendency for C + d to be stronger than E + b ($P = 0.0947$, 1-tailed paired t-test, df = 7). These two averages are significantly different from each other when considering the E + b and C + d synergy coefficients ($P = 0.0083$ by MANOVA, $df = 22$).

The finding of a linkage between D + c caudal extension and C + d entering in the composition of adductions is fortified by other observations. In Fig. 6*A* from a caudal extension site classified as B + e, one caudal extension actually shows compared with the other one the presence of an additional

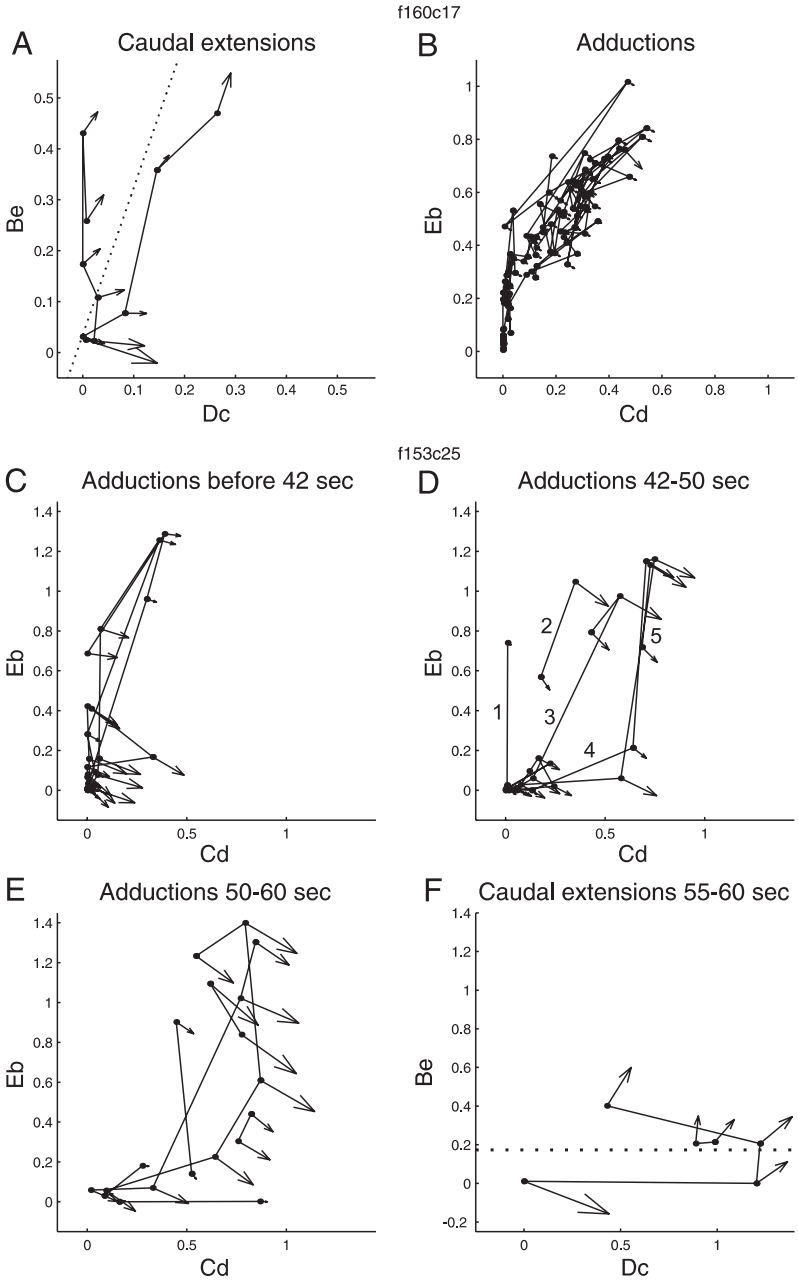

FIG. 6. Further evidence for linkages between caudal extensions and adductions. *A*: 2 caudal extensions (one with 4 and the other with 6 plotted EMG responses, average force direction during each response indicated by arrows with orientation as shown in Fig. 1, *inset*) were obtained from this site (f160c17). Although classified as a Be caudal extension site (perpendicular offset least-squares dotted line; slope, 70.9°; absolute intercept, 2.6%), 1 of 2 caudal extensions (shown in raw data of Fig. 4*A*) clearly has a bit of Dc in addition to Be. Thus there seems to be a core Be to which Dc may be added for caudal extensions from this site. *B*: adductions from the same site as *A*. Note a core Eb component to which Cd may be added, as suggested by the overall spatial distribution of synergy coefficients in the plot. *C–F*: at another site (f153c25), a gradual change in the synergy composition of adductions occurs with time, from Eb without Cd (before 42 s, *C*), to the gradually more important contribution of Cd as shown by successive adductions labeled *1–5* between 42–50 s (*D*) and the overall spatial distribution of synergy coefficients in the plot after 50 s (*E*). When caudal extensions appear in the rhythm at 55 s, they are of the Dc type (least-squares dotted line; slope, 0°; absolute intercept, 14.2%; *F*).

smaller D + c component. At that same site, the adduction responses (Fig. 6*B*) consist of E + b (and A + F + c) to which a smaller C + d component may be added. This example therefore shows a parallel between the addition of D + c in the caudal extension phase and of C + d in the adduction phase. In another example (Fig. 6, *C–F*), adductions early in the rhythm are produced by E + b (Fig. 6*C*). Later in the rhythm, they are progressively produced by a different EMG pattern consisting of C + d together with, and sometimes preceding, E + b in the time course of the individual adduction (Fig. 6, *D* and *E*, contrast with Fig. 6*B*). Soon afterward, D + c caudal extensions appear in the rhythm (Fig. 6*F*). This parallel temporal evolution in the composition of adductions and the appearance of D + c caudal extensions again supports the linkage between D + c in the caudal extension phase and C + d in the adduction phase.

Linkages between caudal extensions and onsets of flexions after caudal extensions

Flexions are typically strong responses involving the coactivation of a large number of muscles (examples of flexion EMG responses are seen immediately after caudal extensions in Figs. 1*B* and 4*A*). This marked coactivation for flexions is confirmed when averaging the coefficients of the same four synergy combinations used to study adductions as they reconstruct the flexions after caudal extensions at B + e and at D + c caudal extension sites. In both cases, all four synergy combinations are activated during the flexions and to a nearly equally important degree [B + e caudal extension sites: A + F + c, 31.9 ± 20.7% (SD); E + b, 26.3 ± 16.6%; C + d, 24.1 ± 18.6%; F + b, 17.6 ± 15.6%; D + c caudal extension sites: A + F + c, 20.7 ± 14.2%; E + b, 23.6 ± 5.3%; C + d, 32.3 ± 16.1%; F + b, 23.5 ± 14.5%].

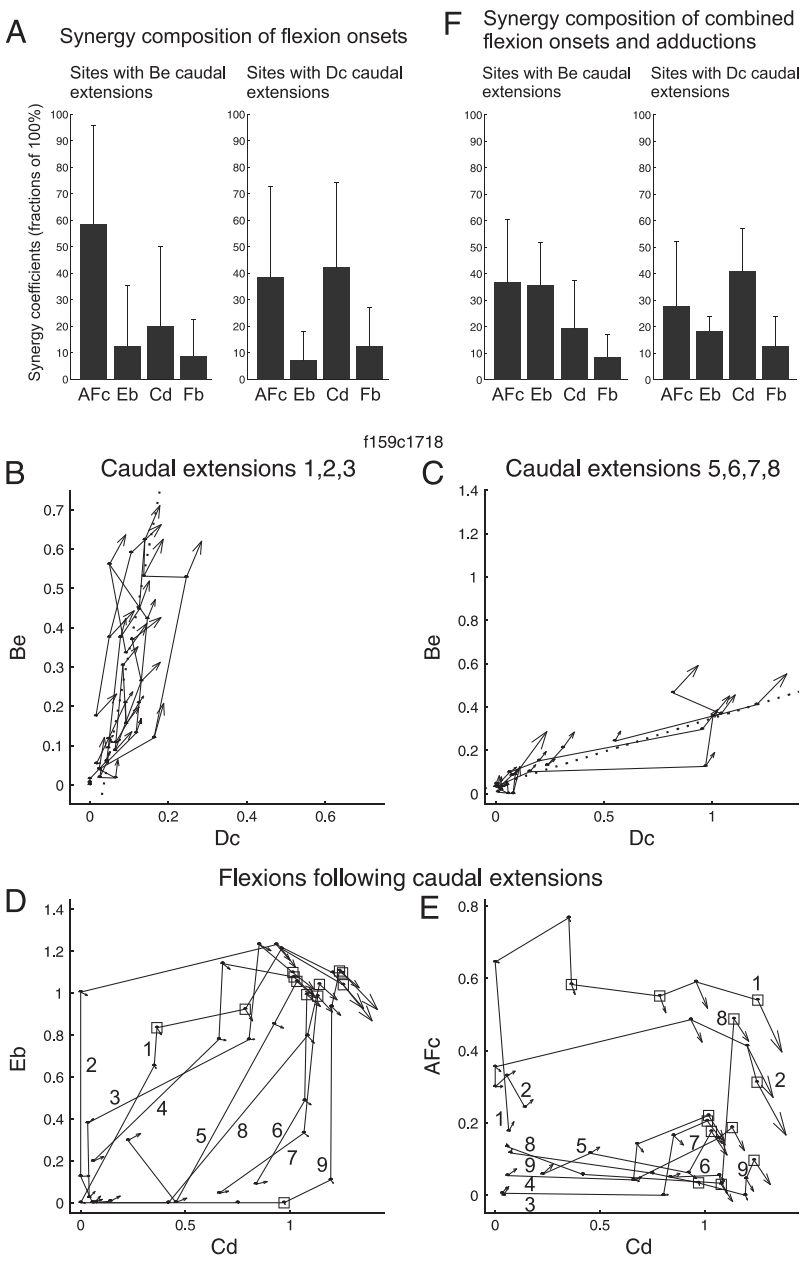

FIG. 7. Linkages between caudal extensions and flexion onsets. *A*: average synergy composition of flexion onsets, expressed in terms of the 4 synergies of Fig. 5*A*, from sites where NMDA-elicited caudal extensions of pure Be or Dc type and also elicited flexions. At each site, the average synergy composition of flexion onset responses was computed and subsequently expressed with the 4 coefficients summing to 100%. Results were averaged for the 2 groups of caudal extension sites (Be, $n = 14$; Dc, $n = 7$). Height of bars indicates average, and thin bars indicate SD. *B* and *C*: caudal extensions from site f159c1718. At this site, caudal extensions followed by flexions were pooled from 2 iontophoretic applications, and the criterion for a caudal extension has been relaxed from $\leq -142.5°$ to $\leq -135°$. The 1st 3 caudal extensions were all of Be type (*B*). The 4th caudal extension (data not shown) was of mixed type. Caudal extensions 5–8 were all of Dc type (*C*). Dotted lines indicate perpendicular offset least-squares fits. Last caudal extension (9; data not shown), although starting with Dc, changed to Be with time and was therefore mixed. *D* and *E*: flexions after caudal extensions 1–9 from the same site. Synergy coefficients are plotted (Eb vs. Cd, *D*; AFc vs. Cd, *E*). Arrows indicate average force direction during each response with the orientation as shown in Fig. 1, *inset*. Squares identify responses where a stable flexion is reached, as flexions develop from caudal extensions, and this helps identify direction of flow within plotted sequences. Number labels 1–9 identify flexions. Beginning with flexion 3, AFc no longer precedes Cd, and with flexion 5, Eb no longer precedes Cd. Thus there is a parallel between change in caudal extension type from Be to Dc and reversal in sequence order for flexions where Cd changes from the last to the 1st activated synergy combination. *F*: average synergy composition of combined flexion onsets and adductions, expressed in terms of the 4 synergies of Fig. 5*A*, from sites where NMDA elicited caudal extensions of pure Be or Dc type and also elicited flexions and adductions (Be, $n = 11$; Dc, $n = 7$). Height of bars indicates average; thin bars indicate SD.

However, another important feature of flexions is that the onsets of muscle activations are not simultaneous but sequential (see Figs. 1*B* and 4*A*). Figure 7*A* shows the averaged coefficients of the same four synergy combinations, as they reconstruct the onsets of flexions at B + e and at D + c caudal extension sites (see METHODS). At B + e caudal extension sites ($n = 14$), the main synergy combination producing the onset of flexion is A + F + c. At D + c caudal extension sites ($n = 7$), the C + d and A + F + c synergy combinations produce the onset of flexion. The greater C + d synergy coefficient for flexion onsets at D + c versus B + e caudal extension sites (Fig. 7*A*) is weakly statistically significant ($P = 0.0672$, 1-tailed *t*-test, $df = 19$).

Again an example of parallel temporal evolution, this time between caudal extensions and the onsets of flexions, supports this linkage (Fig. 7, *B–E*). At this site, caudal extensions early in the rhythm are of the B + e type (Fig. 7*B*) and later change to a D + c type (Fig. 7*C*). In parallel with this, the EMG pattern producing flexions change (Fig. 7, *D* and *E*). Early in the rhythm, flexions begin with A + F + c, preceding E + b and C + d. Later in the rhythm, flexions begin with C + d, preceding E + b and A + F + c. This example shows the linkage between B + e caudal extension and A + F + c flexion onset, being replaced over time by the linkage between D + c caudal extension and C + d in flexion onset.

In summary, in the construction of caudal extension–adduction–flexion rhythms, individual sites tend to produce caudal extensions using either the B + e or D + c synergy combination. In both cases, the synergy combination E + b is key in the production of adduction and the synergy combination A + F + c in bringing about the onset of flexion after caudal extension. A linkage exists between B + e for caudal extension, E + b for adduction, and A + F + c for flexion onset (Figs. 5*C* and 7*A*). In addition, a linkage exists between D + c for caudal exten-

sion and C + d for adduction and flexion onset, in that at D + c caudal extension sites, the C + d synergy combination becomes very important (Figs. 5*C* and 7*A*).

The linkage between caudal extensions and adductions and flexion onsets can also be appreciated by combining the adduction and flexion onset data, because they are reconstructed with the same synergy combinations extracted in Fig. 5*A*. Figure 7*F* shows the average synergy composition of the combined adduction and flexion onset data at the B + e and D + c caudal extension sites where NMDA also elicited both adductions and flexions (see METHODS). There is more A + F + c and E + b for the flexion onset/adduction phases at B + e caudal extension sites and more C + d for these phases at D + c caudal extension sites. These two averages (Fig. 7*F*) are significantly different when considering together the three most activated synergy combinations A + F +c, E + b, and C + d ($P = 0.026$ by MANOVA, $df = 16$).

Topography of caudal extensions and adductions

To study the topography of the key synergy combinations for caudal extensions, we focused on the subset of sites where not only caudal extensions remained of the pure B + e or D + c type, but also where caudal extension represented the initial force elicited by NMDA. The location of these sites, shown in Fig. 8, is clearly different for D + c and B + e. D + c caudal extension maps rostrally about the level of the seventh root. B + e caudal extension primarily maps caudally, especially in the middle of the eighth to ninth segment.

To study the topography of the adductions, we likewise focused on the subset of sites where adduction was the initial force elicited by NMDA. Because we were interested in determining which spinal cord regions may be interconnected to produce different classes of rhythms, we wanted to map where adductions of a synergy composition similar to that of the adductions at B + e caudal extension sites (Fig. 5*C, left*) or to that of the adductions at D + c caudal extension sites (Fig. 5*C, right*) are produced. We therefore divided the sites producing an initial adduction in two groups, using the k-means clustering algorithm, with the synergy compositions shown in Fig. 5*C* defining the initial centers for the clustering (see METHODS). The *left inset* of Fig. 9 shows a histogram of the similarity (measured as the normalized dot product) between the initial adductions of individual sites and these centers. Only 2/23 initial adductions are clearly outliers in that distribution, indicating an atypical synergy composition. Of the other 21 initial adductions, 10 have a synergy composition most similar to that of the adductions at B + e caudal extension sites (mean normalized dot product, 0.92 ± 0.04), and 11 have a synergy composition most similar to that of the adductions at D + c caudal extension sites (mean normalized dot product, 0.90 ± 0.04). After running the k-means clustering algorithm, the 21 sites remained assigned to the same two clusters.

The location of these two groups of initial adductions is shown in Fig. 9. While they do not segregate as clearly as the two types of caudal extensions, a specific region for adductions of a synergy composition typical of rhythms with D + c caudal extensions is the top half of the eighth to ninth segment. Adductions of a synergy composition typical of rhythms with B + e caudal extensions primarily map in the seventh to eighth segment but overlap there with adductions of the other group. Excluding the two very caudal sites in Fig. 9, the initial adductions of type linked to B + e caudal extensions (○) were significantly more rostrally located than the initial adductions of type linked to D + c caudal extensions (●; $0.0326 < P < 0.0394$, 1-tailed Mann-Whitney test; $P = 0.0339$, 1-tailed *t*-test, $df = 17$).

The average composition of the two mapped groups of initial adductions is shown in the *right inset* of Fig. 9. Compared with Fig. 5*C*, the C + d predominance in adductions mapped for their composition typical of rhythms with D + c caudal extensions is now more striking, and the dominance of C + d over E + b is statistically significant ($P = 0.0063$, 1-tailed paired *t*-test, $df = 10$). In addition, we can now appreciate a relatively more important contribution of A + F + c in adductions mapped for their composition typical of rhythms with B + e rather than D + c caudal extensions. This is of interest because rhythms with B + e caudal extensions are also characterized by a dominance of A + F + c in the flexion onsets (Fig. 7*A*) or the combined adduction/flexion onset data (Fig. 7*F*). These results hint that the seventh to eighth segment where adductions linked to B + e caudal extensions map may also be playing a role in flexion onsets in the same rhythms (see DISCUSSION).

Of the 21 mapped sites with initial adductions, NMDA also elicited caudal extensions at 9. Of five sites with initial adduction of a composition expected for a rhythm with B + e caudal extensions, caudal extensions were of B + e type at four and of D + c type at one. Of four sites with initial adduction of a

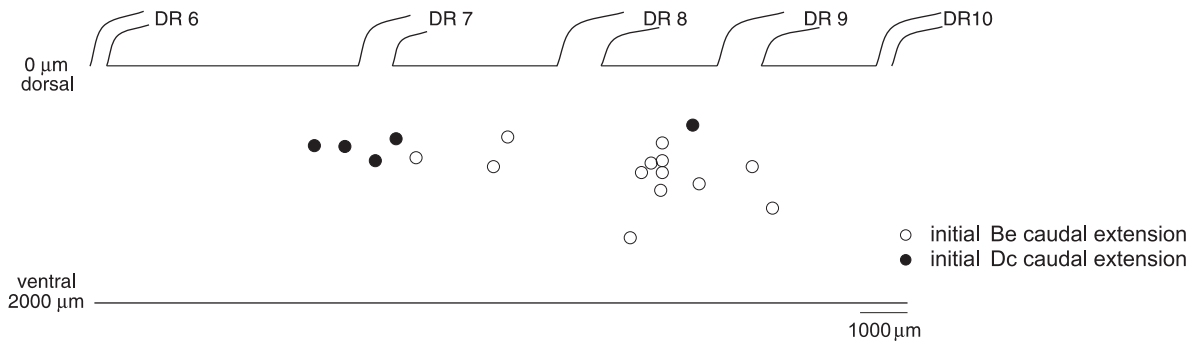

FIG. 8. Topography of the initial caudal extension sites. Lumbar cord is schematized, and dorsal roots 6–10 are labeled. Relative distances between dorsal roots are based on histology measurements from 2 frogs. Sites where NMDA produced a caudal extension as the 1st force and where caudal extensions remained of pure Be or Dc type (according to perpendicular offset least-squares criterion) are mapped. Data source for the maps of Figs. 8–10 include the set of frogs from the histogram of Fig. 3*B* and another set of frogs previously reported (Saltiel et al. 1998).

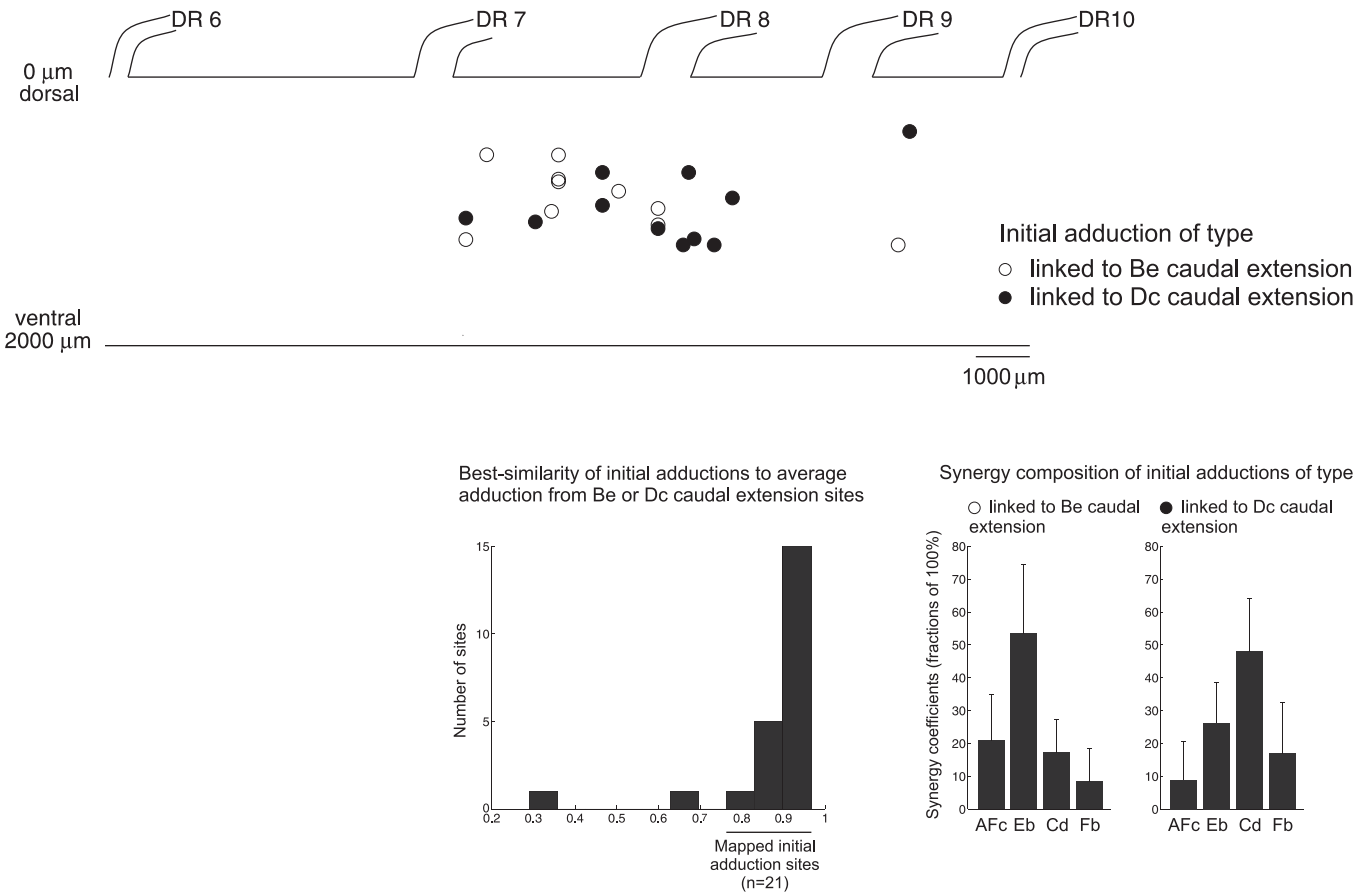

FIG. 9. Topography of the initial adduction sites. *Left inset histogram*: best normalized dot product between synergy composition of initial adductions from individual sites ($n = 23$) and 1 of 2 average synergy compositions of adductions from Be and Dc caudal extension sites of Fig. 5*C*. In this histogram, 2 outliers are evident and not included in the map. The other 21 initial adduction sites are mapped, with 2 different symbols, according to whether synergy composition of their initial adductions clustered with that of adductions from Be or Dc caudal extension sites. *Right inset*: average synergy composition of the 2 mapped groups of initial adductions.

composition expected for a rhythm with D + c caudal extensions, caudal extensions were of D + c type at one, of mixed type but with D + c clearly predominating or preceding B + e in nearly each individual caudal extension at two, and of B + e type at one. This provides further evidence for the linkages in the synergy composition of caudal extensions and adductions.

Given these linkages, we can combine the maps of Figs. 8 and 9, emphasizing now the linked synergy compositions rather than the force direction (Fig. 10). The idea is to visualize and contrast in the same picture which spinal cord regions might be working together to produce the rhythms with the linkages that we have observed.

Topography of linked synergies

In Fig. 10*A*, sites where NMDA elicited initially either an initial caudal extension of the D + c type or an initial adduction of a composition typical of adductions linked to D + c caudal extensions are labeled with ●. Sites where NMDA elicited either an initial caudal extension of the B + e type or an initial adduction of a composition typical of adductions linked to B + e caudal extensions are labeled with ○. It can be seen that these two symbols interleave rostrocaudally as four different regions. ● is found around the level of the seventh root and again in the top half of the eighth to ninth segment. ○ is found in the top two-thirds of the 7th to 8th segment and again in the bottom half of the 8th to 9th segment and top half of the 9th to 10th segment. Boundaries delimiting the four interleaved regions were drawn by visual inspection. Dotted lines indicate some uncertainty for the boundary between the two middle regions.

A similar conclusion of four interleaved regions of ● or ○ predominance is reached when representing each site as a Gaussian centered at the site rostrocaudal location, summing the Gaussians separately for the ● and ○ sites, and plotting these sums along the cord rostrocaudal axis (see METHODS). This is shown in Fig. 10*B*, obtained with a Gaussian width (σ) of 3% of the length of the lumbar cord (from mid-DR6 to mid-DR10), where four major peaks of alternating ● (full curve) or ○ (dashed curve) site predominance are identified at locations similar to the four regions of Fig. 10*A*. The location of the boundaries defined by the intersections of the two curves between the peaks of Fig. 10*B* is reproduced as small full vertical bars at the *bottom* of Fig. 10*A*, and agrees generally well with the boundaries drawn from visual inspection. The exact locations of the intersections slightly depend on σ. Qualitatively however, σ of 3, 2.5, and 2% resulted in the same regional subdivision of sites in the case of the rostral and caudal small vertical bars shown at the *bottom* of Fig. 10*A* for $\sigma = 3\%$. The middle vertical bar subdivision was qualitatively

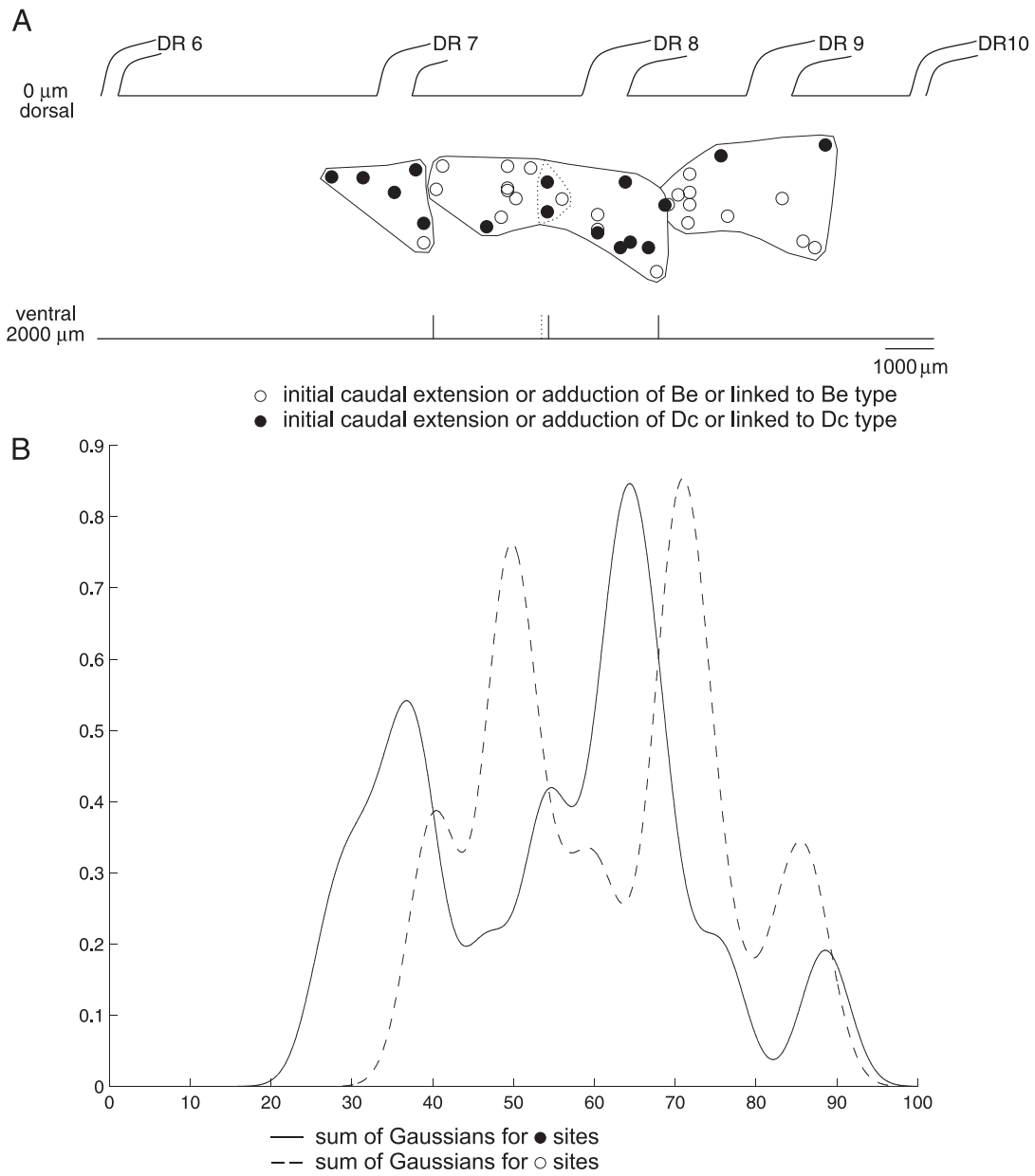

FIG. 10. Topography of linked synergies. *A*: this map is generated by combining maps of Figs. 8 and 9. ●, locations of initial Dc caudal extensions or of initial adductions of the type linked to Dc caudal extensions ($n = 16$); ○, locations of initial Be caudal extensions or of initial adductions of the type linked to Be caudal extensions ($n = 23$). Outlines have been drawn to indicate regions where black or white symbols predominate. Dotted part of outlines indicates uncertainty about the boundary between the 2 middle regions. Small vertical full bars at the *bottom* indicate locations of intersections between peaks in sums of Gaussian curves plotted for ● and ○ sites in *B* ($\sigma = 3\%$ of mid-DR6 to mid-DR10). Small vertical dotted bar at the *bottom* indicates a different middle boundary obtained with $\sigma = 2.5\%$. *B*: after representing each site mapped in *A* as a Gaussian of area equal to 1, sums of Gaussians are computed separately and plotted for ● (full curve) and ○ (dashed curve) sites ($\sigma = 3\%$). Full curve amplitude is normalized to the same number of sites as dashed curve. Abscissa is on the same scale as in *A*, with 0 corresponding to mid-DR6 and 100 to mid-DR10.

similar for $\sigma = 2.5\%$ and $\sigma = 2\%$ (dotted middle bar, shown for $\sigma = 2.5\%$), but slightly different from that for $\sigma = 3\%$ (full middle bar) in that it assigned the two ● sites located a bit above the eighth root to the third instead of the second region from the rostral end.

Having identified these four regions, we can ask whether the degree of ● or ○ predominance between the different regions reaches statistical significance. The boundaries derived from visual inspection (Fig. 10*A*) gave a statistically significant relationship between topography (the 4 regions) and the type of initial synergy composition (● or ○), with a *P* value of 0.0029 or 0.0107 (χ^2, $df = 3$), depending on whether the more rostral or caudal dotted line was taken as the demarcation between the second and third regions. The boundaries derived from Gaussian analysis gave a *P* value of 0.0499 for the 3% Gaussian and of 0.0080 for the 2 and 2.5% Gaussians. Although these results differ slightly from each other because of slight variations in the boundaries, they all indicate a statistically significant relationship between topography and synergy type.

The ● sites represent sites with initial D + c caudal extension or with initial adduction of the type linked to D + c caudal extension. The ○ sites represent sites with initial B + e

caudal extension or with initial adduction of the type linked to B + e caudal extension. The interleaved topographical arrangement of sites that activate synergies observed to be linked in the rhythms emphasizes that rhythms may be constructed preferentially from linkages between distant rather than adjacent spinal cord regions.

DISCUSSION

Evidence for modularity from EMG patterns and their linkages

One of the main results of this paper is that caudal extensions EMG patterns were of two major types, determined by two distinct synergy combinations (B + e and D + c), and this type tended to remain the same throughout the entire rhythm elicited by NMDA at a given site (Fig. 3, *A* and *B*). This was true, although rhythms that included caudal extensions could be obtained from sites in different cord regions (e.g., the sites of Fig. 8 and several of those of Fig. 9, as well as others not shown in these maps restricted to initial caudal extensions and adductions). This already suggests, before any topographic mapping, that there could be two obligatory premotor regions encoding caudal extensions, i.e., regions whose activation would be required for caudal extension to appear as part of the motor output. That in general the two types of caudal extensions are not mixed in individual rhythms further suggests that individual sites where NMDA elicited caudal extensions as part of the output are preferentially connected to one or the other of these putative premotor regions. Recent work on second-order vestibular neurons also suggests that the vestibular circuitry is organized as a premotor rather than a sensory map (Straka et al. 2003).

If there are preferential projections to one of two caudal extension premotor regions, one might expect them to originate from different populations of sites. One way to examine for this, again before any topographic mapping, is to verify whether sites that produce one versus the other type of caudal extension as part of the NMDA-elicited output, also differ in terms of the EMG patterns producing the other force phases typical of rhythms with caudal extensions, i.e., adductions and flexions. We did find this to be the case. At sites where caudal extension sites elicited by NMDA are of the B + e type, adductions are mainly produced by the synergy combination E + b (Fig. 5*C, left*), and the flexions after caudal extensions begin with the synergy combination A + F + c (Fig. 7*A*, *left*). At sites where caudal extension sites elicited by NMDA are of the D + c type, the synergy combinations underlying adductions and flexion onsets still include E + b, and A + F + c, respectively, but the synergy composition of both phases now includes an important C + d component (Figs. 5*C, right*, and 7*A, right*).

In summary, these results support modularity of the spinal cord, with two distinct modules available to produce caudal extensions. In addition, examination of the synergy composition of the other phases of the rhythms with caudal extensions suggests that different modules also exist for adductions that are linked in a specific way to the modules producing caudal extensions to produce the observed linkages in the EMG patterns and their underlying synergy combinations.

Evidence for modularity from topography

Sites where NMDA elicited a B + e versus D + c caudal extension as the initial response and where subsequent caudal extensions remained of the same type during the rhythm map to distinct spinal cord regions whose centers are far apart along the rostrocaudal axis (mid 8th to 9th segment and 7th root level, respectively, Fig. 8). An earlier study with NMDA where we had mapped sites eliciting a single tonic force of constant direction had already hinted at these two regions for producing caudal extensions (Saltiel et al. 1998). The results in this paper clearly indicate that the encoding of a distinct synergy combination producing a caudal extension force corresponds to each of these regions.

Mapping the sites producing an initial adduction force of a synergy composition typical of the adduction phase in rhythms with either B + e or D + c caudal extension also shows a topographic organization of these two types of adduction, significantly although not as fully segregated as for the caudal extensions (Fig. 9). The regions for the two types of adductions are approximately adjacent, with some overlap, and together are located between the caudal extension regions. In particular, the region in the top half of the eighth to ninth segment encodes rather specifically adductions of a synergy composition typical of rhythms with D + c caudal extensions.

The region of adduction as the initial response in Fig. 9 includes, but is larger than, the area where we previously mapped sites producing a tonic adduction force. Initial adductions of the type linked to B + e caudal extensions extend more rostrally in the seventh to eighth segment into the area where we previously mapped sites producing a tonic rostral flexion force (Saltiel et al. 1998). This may not be completely surprising given that *1*) adductions linked to B + e caudal extensions appear to have a relatively more important contribution of A + F + c than the other group of adductions (Fig. 9, *right inset*) and *2*) A + F + c is a key synergy combination for flexion onsets, particularly for B + e caudal extension rhythms (Fig. 7*A, left*). Thus it is conceivable that the area where adductions linked to B + e caudal extensions map may also be playing a role in flexion onsets in the same rhythms. In that sense, it may not be surprising that this area, located in the seventh to eighth segment (Fig. 9, ○), overlaps the area where we previously mapped sites producing a tonic rostral flexion force.

Comparison with another modular view of the spinal cord and considering alternative interpretations to modularity

A detailed study of the organization of nociceptive withdrawal reflexes in the rat and cat has revealed modules at the single muscle level, whereby the cutaneous receptive field of any given muscle strikingly corresponds to the area of skin maximally withdrawn by contraction of that muscle (Schouenborg 2002). Candidate reflex-encoder interneurons with cutaneous receptive fields similar to that of individual muscles exist in the deep dorsal horn (27/147 lamina V interneurons; Levinsson et al. 2002; Schouenborg et al. 1995). These results are difficult to compare with ours because they focus on single muscles rather than groups of muscles (synergies), even though it is clear that the cutaneous receptive fields of individual muscles partially overlap (Schouenborg and Kalliomäki 1990). It might be interesting to know among the 120/147 lamina V

interneurons with cutaneous receptive fields different from those of single muscles, whether some had receptive fields corresponding to the overlapping region shared by a pair or group of muscles, or whether some had receptive fields limited to the nonshared region unique to a given muscle. The existence of the former type of interneuron might support the encoding of synergies grouping the muscles with overlapping receptive fields. The existence of the latter type of interneuron might also be relevant to our results where one adduction pattern consists mostly of E + b by itself, in contrast to the other adduction pattern that activates C + d in addition to E + b (Fig. 5*C*). In the work on withdrawal reflexes, the motor output targets of the lamina V interneurons have not been directly studied. It is noteworthy that one place where inputs as single muscle withdrawal modules may somehow be transformed to multi-joint synergies, a modular view closer to ours, is the cerebellum (Garwicz 2002; Garwicz et al. 2002).

The view of spinal cord modularity presented in our paper does find support in an important way in the work of Schouenborg et al. on one precise point. Whereas the muscles activated in the nociceptive withdrawal reflexes are largely flexor, the extensor GA can be activated from heel stimulation. Mapping primary afferents from that cutaneous region reveals a unique termination pattern, in that not one, but two distinct regions are labeled in the rat spinal cord, i.e., caudally at mid-L_5 and rostrally at mid-L_3 (Levinsson et al. 2002). This is interesting because GA (synergy A, see Fig. 2) is precisely the synergy shared by our two caudal extension EMG patterns that also map at two distinct locations, the pattern defined by B + e, which maps caudally, and the pattern defined by D + c, which maps rostrally (Fig. 8).

We may also ask whether our results could be interpreted in other ways than according to a modular hypothesis. Morton and Chiel (1994) suggested three possible neural architectures for adaptive behavior: dedicated circuitry; distributed circuitry; and reorganizing circuitry. They cautioned that many biological circuit examples simultaneously showed features of the different architectures. Distributed circuitry is characterized by a continuum of responses in the motor output and by a single population of neurons being used for all responses (Morton and Chiel 1994). In the case of the caudal extension patterns, the distinctly different synergy combinations B + e and D + c, the finding that they are rarely mixed, i.e., do not form a continuum (Fig. 3*B*), and their distinct topography, suggesting distinct interneuron populations (Fig. 8), support a dedicated (modular) circuitry and not distributed circuitry. At the same time, the shared synergy A may suggest a feature of reorganizing circuitry, in that synergy A may actually be combined with synergy B + e or with synergy D + c, i.e., made part of one or the other caudal extension pattern.

In the case of the adductions, the fact that there is little C + d in the adductions linked to B + e caudal extensions compared with the strong or predominant C + d in the adductions linked to D + c caudal extensions (Figs. 5*C* and 9, *right inset*) is against a continuum of responses. Furthermore, the interneurons of the more caudal adduction region in Fig. 9 (where ● sites producing initial adductions with C + d predominance are mainly located) are unlikely to be recruited during the production of adductions of the type linked to B + e caudal extensions, because the latter adductions have little C + d. Together these two arguments against a continuum of responses and against a single interneuronal population (the entire initial adduction zone in Fig. 9) being recruited whenever an adduction is produced are against distributed circuitry. It remains possible that interneurons of the more rostral adduction region in Fig. 9 (where ○ sites producing initial adductions consisting primarily of E + b are mainly located) might be recruited by the more caudal adduction region during the production of adductions of the type linked to D + c caudal extensions (adductions with both C + d and E + b) to obtain the E + b component. However, even if this was the case, it would still imply dedicated circuitry, the more rostral adduction region being necessary to obtain E + b and the more caudal adduction region to obtain C + d.

Thus it seems that the results about the synergy combinations underlying the caudal extensions and adductions, their topography, and the observed linkages all reinforce each other to suggest a modular architecture.

Functional considerations about spinal modular circuits and their connectivity in a topographic context

The overall topographic organization is perhaps best appreciated in the combined map of caudal extensions and adductions (Fig. 10). As indicated in RESULTS, this map builds over the linkages described in the previous section by lumping together the initial caudal extensions and adductions belonging to the same linked group and representing them as a single symbol. In this map, one can appreciate the interleaving of the two symbols in four sequential regions along the rostrocaudal axis. The force produced by the two middle regions is typically an adduction and by the most rostral and caudal regions is typically a caudal extension. Thus if we represent the symbol by a digit, we would have along the rostrocaudal axis CE2-ADD1-ADD2-CE1, with CE2 the label for the most rostral region in Fig. 10. Our observations suggest that CE2 and ADD2 are linked to produce the rhythm with D + c caudal extensions, and the adductions of the type typically associated with them. CE1 and ADD1 are linked to produce the rhythm with B + e caudal extensions, and the adductions of the type typically associated with them. This map emphasizes that distant rather than immediately adjacent regions are preferentially linked in the construction of rhythms.

It is quite conceivable that in some cases NMDA was applied at the border between two adjacent regions (e.g., ADD2 and CE1), and this may in part account for individual examples where the usual linkages were not found. In support of this interpretation is the type of mislinkages we observed when we averaged separately the four synergy coefficients reconstructing all of the adduction EMG responses from each site with adductions, clustered these averages in a way similar to the analysis for Fig. 9, and determined for the subset of sites also producing caudal extensions whether these were of B + e (CE1) or D + c (CE2) type. We found that of 14 sites with adductions of the ADD1 type, caudal extensions were of the CE1 type at 12, of CE2 type at 1, and mixed at 1, and that of 13 sites with adductions of the ADD2 type, caudal extensions were of the CE2 type at 10, and of CE1 type at 3 (data not shown). Thus in agreement with an interpretation of mislinkages based on a closer anatomical proximity of the underlying modules, mislinkages were more often observed between ADD2 and CE1 (which are closer peaks in Fig. 10*B*) than

between ADD1 and CE2. More generally, we cannot exclude the possibility that the modules may be less segregated than we found in Fig. 10, perhaps with a finer interdigitating substructure or that interneurons encoding ADD2 and CE1 are partially mixed topographically or weakly interconnected. Overall, however, Fig. 10, together with the linkages, does suggest two specifically interconnected CE-ADD systems (CE1-ADD1 and CE2-ADD2), which are topographically organized as four interleaved regions rather than indiscriminately mixed. Other arguments supporting modularity have been indicated in the previous section.

The proximity of ADD1 and ADD2 as opposed to the distance between CE1 and CE2 makes it also understandable that it is easier to separate these two systems by focusing first on the caudal extensions and later on the adductions, as we have done in our analysis. In some cases, caudal extensions changed in type during a rhythm. Although this may in part reflect imperfections of the NMDA technique such as border applications, it also suggests that these two systems (CE1-ADD1 and CE2-ADD2) are not necessarily always operating in isolation from each other. Even in these more complex cases, the linkages were respected (Figs. *6* and 7, *B–E*). This provides reassurance about the functional nature of our observations with NMDA.

A more detailed consideration of the linked synergy combinations may also provide more insight about how the linked regions in Fig. 10 might operate. The key synergy combination in CE1 is B + e, whereas the key synergy combination for ADD1 is E + b. The key synergy combination in CE2 is D + c, whereas the dominant synergy combination for ADD2 is C + d (although there is also activation of E + b). Thus for both linked systems, the two phases of caudal extensions and adductions share synergies, with one or the other more strongly expressed depending on the phase. One must therefore definitely consider the possibility that the linked regions, e.g., CE1 and ADD1, do not function in a strictly reciprocal fashion, being active only during the corresponding force phase. Interneurons projecting from one linked region to another are likely essential for the construction of the rhythm. Thus the region mapped as CE1 for example may well contain different classes of interneurons, among which premotor interneurons encoding the B synergy, and another population of interneurons projecting to the distant ADD1 region, which in turn would comprise interneurons encoding the E synergy. This would represent a more parsimonious synergy mapping, i.e., B and not B + e for CE1, whereas B + e would appear as the synergy combination on stimulating CE1 because of the connectivity between the linked regions.

The two main findings of our paper, that different synergy combinations can be obtained from distinct regions of the lumbar spinal cord, and there are specific linkages between these regions, resemble issues in research on motor cortex organization. On the one hand, it has become clear that small regions of motor cortex can activate muscle combinations, ~6 ± 4 muscles, as revealed by spike-triggered or stimulus-triggered averages (Cheney and Fetz 1985; McKiernan et al. 2000; Park et al. 2004). Within the forelimb area of motor cortex, there is a topographic organization to these muscle combinations, with a region activating both proximal and distal muscles, located between a region activating distal muscles only, and a region activating proximal muscles only (Park et al. 2001). The concept of different combinations of muscle activations evoked from different regions (see also Schieber 2001) is similar to the first finding in our paper. On the other hand, there are also intrinsic horizontal connections within the forelimb area of motor cortex, which connect sites evoking movements at the same or different forelimb joints (Huntley and Jones 1991). The organization is imperfectly understood, in part because the interconnected sites have generally been mapped only in terms of which joint moved on site stimulation, without further details about the movement direction or the activated EMGs. One study showed the pattern of interconnections to include motor cortical sites evoking antagonist EMGs and movements at the wrist joint (Capaday et al. 1998). What seems clear, however, is that these connections are between patches as revealed by anterograde and retrograde labeling studies (Huntley and Jones 1991). Their suggested role has been to link together different segments of a complex movement (Aroniadou and Keller 1993; Keller 1993). The concept of interconnected patches and the idea that they may relate to different phases of a movement is similar to the second finding in our paper of linkages between specific spinal cord regions constructing together the different phases of a rhythm. Furthermore, although the population code of the motor cortex, whereby the direction of arm movement would arise from the weighted sum of activities of cells with different preferred directions (Georgopoulos et al. 1982), is considered a traditional example of distributed circuitry, recent results directly support a modular architecture of the motor cortex (Amirikian and Georgopoulos 2003). Cells with the same preferred direction cluster in vertical minicolumns 50–100 μm wide, which may repeat 200 μm apart, and are interleaved with minicolumns of the nearly orthogonal preferred direction. Columns of nearly opposite preferred direction cluster 350 μm apart.

One may also relate our results to emerging principles of cerebellar function (Apps and Garwicz 2005; Ekerot and Jörntell 2003). In the cat, mossy fibers with a given cutaneous receptive field project to a cerebellar microzone where, through local granule cells activating local inhibitory interneurons, they locally inhibit Purkinje cells. This releases cerebellar nuclear neurons, resulting in a movement that will typically withdraw the cutaneous receptive field from contact. On the other hand, excitation of the same Purkinje cells, which will inhibit the output from the microzone, arises not locally, but from parallel fibers of distant granule cells activated by another set of mossy fibers with a different cutaneous receptive field and terminating in a *distant* microzone. This led to suggest that the two sets of mossy fibers may be linked functionally, so that the movement resulting from the activation of the first set of mossy fibers may lead to stimulation of the second set of mossy fibers, resulting in inhibition of the movement induced by the first set of mossy fibers, and the onset of another movement. This might in theory happen as well with other inputs such as group II muscle afferent inputs or central inputs conveyed by mossy fibers.

This general idea resembles our results about how modularity and interconnectivity between modules may be important in the control of a sequence of movements or a rhythm. It may also provide a framework for recent results demonstrating discrete shifts in the duration of EMG burst components exerted at critical points in the fictive forelimb locomotor cycle by tonic proprioceptive inputs, in the decerebrate cat with the cerebellum intact (Saltiel and Rossignol 2004).

Possible implications for construction of natural behaviors and their supraspinal/afferent control

Our results on spinal cord topographic organization may also provide insight into whether or not specific supraspinal and afferent inputs will or will not influence the control of different natural motor behaviors. To illustrate this, we will focus on the result of two distinct caudal extension regions in the frog lumbar spinal cord.

In the cat, experiments designed to study the functional organization of the extensor half-center, believed to generate the stance phase of locomotion, have suggested that it comprises two different groups of interneurons (Leblond et al. 2000; see Introduction). Several segmental and supraspinal pathways are known to excite extensor motoneurons, including contralateral flexor muscle afferents (co FRA), group I afferents from knee and ankle extensor muscles (this latter pathway reverses sign to excitatory during locomotion), vestibulospinal inputs from Deiter's nucleus (DN), and reticulospinal inputs from the medial longitudinal fasciculus (MLF). Spatial facilitation experiments aimed at elucidating whether these different inputs converge on the same or separate interneurons have suggested the following two groups of extensor interneurons; one group is co-activated by co FRA, MLF and group I afferents from extensor muscles inputs, while the other group is co-activated by co FRA and DN inputs (Gossard et al. 1996; Leblond and Gossard 1997; Leblond et al. 2000). These two putative groups of spinal interneurons have not been directly mapped. Still it is interesting that the group I afferents from knee/ankle extensors and the vestibular (DN) inputs, which through their lack of convergence define the two groups of extensor interneurons, respectively appear to project caudally and rostrally in the lumbar cord (Gossard et al. 1994; Krutki et al. 2003; Kuze et al. 1999; Loeb et al. 1985). This is reminiscent of our two regions encoding caudal extension in the frog spinal cord.

In the frog, various results suggest how these two regions could be used to construct the extensions of natural behaviors, and for their descending and/or afferent control. From work extracting synergies from natural behaviors, the two main synergies that may enter in the composition of swimming extension EMGs are similar to the patterns encoded by our rostral and caudal lumbar caudal extension regions, with the rostral lumbar region pattern dominating. In contrast, jumping extension EMGs are primarily produced by a synergy similar to the pattern encoded by our caudal lumbar caudal extension region (A.d'A., unpublished observations; Cheung et al. 2005). The anatomical details of the vestibulospinal projections are less well known in the frog than in the cat (Matesz et al. 2002). However among the synergies extracted from responses to whole-body rotations in the frog, one resembles the D synergy, but none resembles the B synergy, which may constitute evidence of a vestibular projection to the rostral lumbar caudal extension region (d'Avella 2000). Vestibular inputs are crucial in lamprey swimming (Deliagina 1997; Deliagina and Pavlova 2002), and appear similarly important in frog swimming (J. Schotland, personal communication). In the frog, hindlimb extensor muscle afferents are expected to enter the cord through the dorsal eighth and ninth lumbar roots (Dunn 1900), and thus at the level of the caudal, but not of the rostral lumbar caudal extension region. One could therefore tentatively suggest that swimming extensions are produced primarily by the rostral lumbar caudal extension region, which would be under vestibular, but not under extensor muscle afferent control. While jumping extensions would be produced primarily by the caudal lumbar caudal extension region, that would be under extensor muscle afferent control. In support of this is the result that deafferentation (transection of the dorsal lumbar roots) has a greater effect on the jumping than on the swimming extension EMGs (Cheung et al. 2005).

In conclusion, we believe that the use of a reduced spinal preparation, together with the method of focal NMDA application, allows to dissect basic building blocks of the neural circuitry of motor behavior, and to provide functional insight in their connectivity. Furthermore, this insight can be mapped topographically onto the spinal cord and guide future recording, anatomical, lesion and genetic studies.

ACKNOWLEDGMENTS

We thank V.C.K. Cheung for help with computing the angle between vectors in four-dimensional space and M. Cantor and S. Szczepanowski for technical support.

GRANTS

This work was supported by National Institute of Neurological Disorders and Stroke Grant NS-09343 to E. Bizzi and the Swiss National Science Foundation to K. Wyler-Duda.

REFERENCES

Amirikian B and Georgopoulos AP. Modular organization of directionally tuned cells in the motor cortex: is there a short-range order? *Proc Natl Acad Sci USA* 100: 12474–12479, 2003.

Apps R and Garwicz M. Anatomical and physiological foundations of cerebellar information processing. *Nat Rev Neurosci* 6: 297–311, 2005.

Aroniadou VA and Keller A. The patterns and synaptic properties of horizontal intracortical connections in rat motor cortex. *J Neurophysiol* 70: 1553–1569, 1993.

Berkowitz A. Broadly tuned spinal neurons for each form of fictive scratching in spinal turtles. *J Neurophysiol* 86: 1017–1025, 2001a.

Berkowitz A. Rhythmicity of spinal neurons activated during each form of fictive scratching in spinal turtles. *J Neurophysiol* 86: 1026–1036, 2001b.

Bertrand S and Cazalets JR. The respective contribution of lumbar segments to the generation of locomotion in the isolated spinal cord of the newborn rat. *Eur J Neurosci* 11: 583–592, 2002.

Butt SJB and Kiehn O. Functional identification of interneurons responsible for left-right coordination of hindlimbs in mammals. *Neuron* 38: 953–963, 2003.

Capaday C, Devanne H, Bertrand L, and Lavoie BA. Intracortical connections between motor cortical zones controlling antagonistic muscles in the cat: a combined anatomical and physiological study. *Exp Brain Res* 120: 223–232, 1998.

Cheney PD and Fetz EE. Comparable patterns of muscle facilitation evoked by individual corticomotoneuronal (CM) cells and by single intracortical microstimuli in primates: evidence for functional groups of CM cells. *J Neurophysiol* 53: 786–804, 1985.

Cheng J, Jovanovic K, Aoyagi Y, Bennett DJ, Han Y, and Stein RB. Differential distribution of interneurons in the neural networks that control walking in the mudpuppy (Necturus maculatus) spinal cord. *Exp Brain Res* 145: 190–198, 2002.

Cheng J, Stein RB, Jovanovic K, Yoshida K, Bennett DJ, and Han Y. Identification, localization, and modulation of neural networks for walking in the mudpuppy (Necturus maculatus) spinal cord. *J Neurosci* 18: 4295–4304, 1998.

Cheung VCK, d'Avella A, Tresch MC, and Bizzi E. Central and sensory contributions to the activation and organization of muscle synergies during natural motor behaviors. *J Neurosci* 25: 6419–6434, 2005.

d'Avella A. *Modular Control of Natural Behavior* (PhD thesis). Cambridge, MA: Massachusetts Institute of Technology, 2000.

Deliagina T. Vestibular compensation in lampreys: impairment and recovery of equilibrium control during locomotion. *J Exp Biol* 200: 1459–1471, 1997.

Deliagina TG and Pavlova EL. Modifications of vestibular responses of individual reticulospinal neurons in lamprey caused by unilateral labyrinthectomy. *J Neurophysiol* 87: 1–14, 2002.

Dunn EH. The number and size of the nerve fibers innervating the skin and muscles of the thigh in the frog (Rana Virescens Brachycephala, Cope). *J Comp Neurol* 10: 218–242, 1900.

Ekerot CF and Jörntell H. Parallel fiber receptive fields: a key to understanding cerebellar operation and learning. *Cerebellum* 2: 101–109, 2003.

Garwicz M. Spinal reflexes provide motor error signals to cerebellar modules. *Brain Res Rev* 40: 152–165, 2002.

Garwicz M, Levinsson A, and Schouenborg J. Common principles of sensory encoding in spinal reflex modules and cerebellar climbing fibres. *J Physiol* 540: 1061–1069, 2002.

Georgopoulos AP, Kalaska JF, Caminiti R, and Massey JT. On the relations between the direction of two-dimensional arm movements and cell discharge in primate motor cortex. *J Neurosci* 2: 1527–1537, 1982.

Gossard JP, Brownstone RM, Barajon I, and Hultborn H. Transmission in a locomotor-related group Ib pathway from hindlimb extensor muscles in the cat. *Exp Brain Res* 98: 213–228, 1994.

Gossard JP, Floeter MK, Degtyarenko AM, Simon ES, and Burke RE. Disynaptic vestibulospinal and reticulospinal excitation in cat lumbosacral motoneurons: modulation during fictive locomotion. *Exp Brain Res* 109: 277–288, 1996.

Hartigan JA and Wong MA. A k-means clustering algorithm. *Appl Stat* 28: 100–108, 1979.

Huntley GW and Jones EG. Relationship of intrinsic connections to forelimb movement representations in monkey motor cortex: a correlative anatomic and physiological study. *J Neurophysiol* 66: 390–413, 1991.

Keller A. Intrinsic connections between representation zones in the cat motor cortex. *Neuroreport* 4: 515–518, 1993.

Kjaerulff O and Kiehn O. Distribution of networks generating and coordinating locomotor activity in the neonatal rat spinal cord in vitro. A lesion study. *J Neurosci* 16: 5777–5794, 1996.

Krutki P, Jankowska E, and Edgley SA. Are crossed actions of reticulospinal and vestibulospinal neurons on feline motoneurons mediated by the same or separate commissural neurons? *J Neurosci* 23: 8041–8050, 2003.

Kuze B, Matsuyama K, Matsui T, Miyata H, and Mori S. Segment-specific branching patterns of single vestibulospinal tract axons arising from the lateral vestibular nucleus in the cat: a PHA-L study. *J Comp Neurol* 414: 80–96, 1999.

Leblond H and Gossard JP. Supraspinal and segmental signals can be transmitted through separate spinal cord pathways to enhance locomotor activity in extensor muscles in the cat. *Exp Brain Res* 114: 188–192, 1997.

Leblond H, Ménard A, Gossard JP. Bulbospinal control of spinal cord pathways generating locomotor extensor activities in the cat. *J Physiol* 525: 225–240, 2000.

Levinsson A, Holmberg H, Broman J, Zhang M, and Schouenborg J. Spinal somatosensory transformation: relation between cutaneous somatotopy and a reflex network. *J Neurosci* 22: 8170–8182, 2002.

Loeb EP, Giszter SF, Saltiel P, Mussa-Ivaldi FA, and Bizzi E. Output units of motor behavior: an experimental and modeling study. *J Cogn Neurosci* 12: 78–97, 2000.

Loeb GE, Hoffer JA, and Pratt CA. Activity of spindle afferents from cat anterior thigh muscles. I. Identification and patterns during normal locomotion. *J Neurophysiol* 54: 549–564, 1985.

Marcoux J and Rossignol S. Initiating or blocking locomotion in spinal cats by applying noradrenergic drugs to restricted lumbar spinal segments. *J Neurosci* 20: 8577–8585, 2000.

Matesz C, Kulik A, and Bácskai T. Ascending and descending projections of the lateral vestibular nucleus in the frog Rana esculenta. *J Comp Neurol* 444: 115–128, 2002.

McKiernan BJ, Marcario JK, Karrer JH, and Cheney PD. Correlations between corticomotoneuronal (CM) cell postspike effects and cell-target muscle covariation. *J Neurophysiol* 83: 99–115, 2000.

Morton DW and Chiel HJ. Neural architectures for adaptive behavior. *Trends Neurosci* 17: 413–420, 1994.

Park MC, Belhaj-Saïf A, and Cheney PD. Properties of primary motor cortex output to forelimb muscles in rhesus macaques. *J Neurophysiol* 92: 2968–2984, 2004.

Park MC, Belhaj-Saïf A, Gordon M, and Cheney PD. Consistent features in the forelimb representation of primary motor cortex in rhesus macaques. *J Neurosci* 21: 2784–2792, 2001.

Saltiel P and Rossignol S. Critical points in the forelimb fictive locomotor cycle and motor coordination: evidence from the effects of tonic proprioceptive perturbations in the cat. *J Neurophysiol* 92: 1329–1341, 2004.

Saltiel P, Tresch MC, and Bizzi E. Spinal cord modular organization and rhythm generation: an NMDA iontophoretic study in the frog. *J Neurophysiol* 80: 2323–2339, 1998.

Saltiel P, Wyler-Duda K, d'Avella A, Tresch MC, and Bizzi E. Muscle synergies encoded within the spinal cord: evidence from focal intraspinal NMDA iontophoresis in the frog. *J Neurophysiol* 85: 605–619, 2001.

Schieber MH. Constraints on somatotopic organization in the primary motor cortex. *J Neurophysiol* 86: 2125–2143, 2001.

Schouenborg J. Modular organization and somatosensory imprinting. *Brain Res Rev* 40: 80–91, 2002.

Schouenborg J and Kalliomäki J. Functional organization of the nociceptive withdrawal reflexes. I. Activation of hindlimb muscles in the rat. *Exp Brain Res* 83: 67–78, 1990.

Schouenborg J, Weng HR, Kalliomäki J, and Holmberg H. A survey of spinal dorsal horn neurons encoding the spatial organization of withdrawal reflexes in the rat. *Exp Brain Res* 106: 19–27, 1995.

Stein PSG and Daniels-McQueen S. Modular organization of turtle spinal interneurons during normal and deletion fictive rostral scratching. *J Neurosci* 22: 6800–6809, 2002.

Stein PSG and Daniels-McQueen S. Variations in motor patterns during fictive rostral scratching in the turtle: knee-related deletions. *J Neurophysiol* 91: 2380–2384, 2004.

Straka H, Holler S, Goto F, Kolb FP, and Gilland E. Differential spatial organization of otolith signals in frog vestibular nuclei. *J Neurophysiol* 90: 3501–3512, 2003.

Tresch MC, Saltiel P, and Bizzi E. The construction of movement by the spinal cord. *Nat Neurosci* 2: 162–167, 1999.

Tresch MC, Saltiel P, d'Avella A, and Bizzi E. Coordination and localization in spinal motor systems. *Brain Res Rev* 40: 66–79, 2002.

Tukey JW. *Exploratory Data Analysis.* Reading, MA: Addison-Wesley, 1977.

Weisstein EW. *Gaussian Function*. Available online at http://mathworld.wolfram.com/GaussianFunction.html. [4 Nov. 2004].

Weisstein EW. *Least Squares Fitting—Perpendicular Offsets.* Available online at http://mathworld.wolfram.com/LeastSquaresFittingPerpendicularOffsets.html. [2 Apr. 2003].